

U N I V E R S I T E
BLAISE PASCAL
C L E R M O N T - F E R R A N D

AGV for agricultural and green space field

Philippe Martinet ^a

2 September 1997

LASMEA

Blaise Pascal University

63177 Aubière cedex

LASMEA

P. Bonton, J. Gallice, D. Khadraoui



Institut de recherche
pour l'ingénierie
de l'agriculture
et de l'environnement

Cemagref Clermont-Ferrand

M. Berducat, C. Debain, M. Derras, R. Rouveure

^aemail: martinet@lasmea.univ-bpclermont.fr

Contents

1	Introduction	4
2	About the vision aspect	8
2.1	Introduction	8
2.2	Our Approach	10
3	AGV in green space environment	13
3.1	Introduction	16
3.2	Modelling of the Scene	17
3.3	Trajectory generation	22
3.4	Results	27
4	AGV in agricultural field	32
4.1	Introduction	32
4.2	Modelling of the Scene	36
4.3	Control Aspect	39
4.3.1	Task Function Approach	40
4.3.2	Neural Approach	53
4.4	Experimental Results	61
4.4.1	Implementation Considerations	61
4.4.2	First Law	64

4.4.3	Second Law	67
4.4.4	Third Law (neural approach)	70
4.4.5	Conclusion	73
4.5	Guiding the vehicle on a slope ground . . .	75
5	Conclusion and Perspectives	82
6	Video	84

1 Introduction

Many guiding applications :

Figure 1: Green space environment (Mower)

Figure 2: Harvesting context (Combine harvester)

Many guiding applications (next) :

Figure 3: Tillage and Baler applications (Tractor)

Figure 4: Machine for multi-applications (Articulated tractor)

Environment considerations :

- structured (generally indoor)
- unstructured (generally outdoor)

In these applications the environment is partially structured and characterised by :

- initial path
- guiding/following path

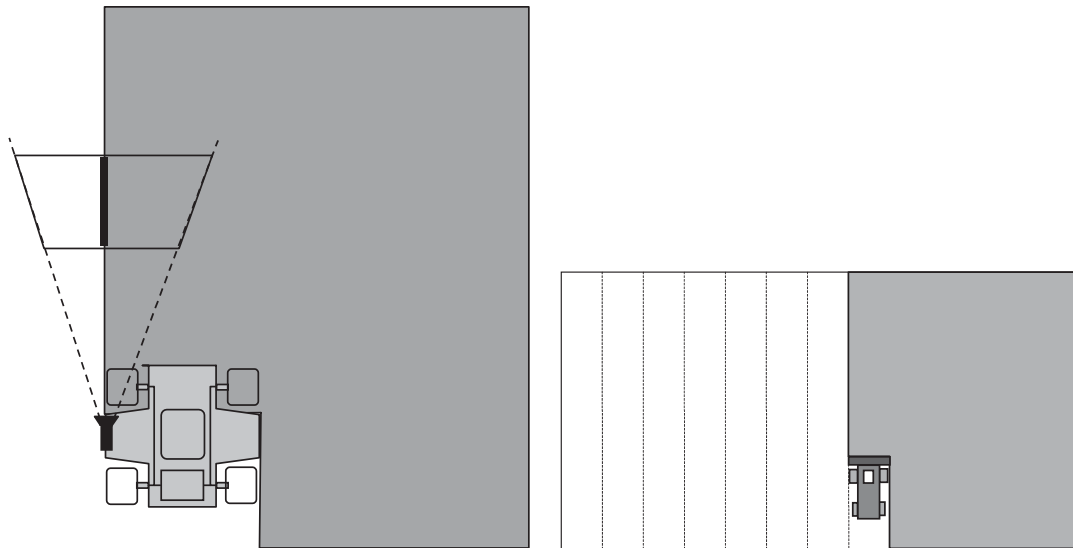


Figure 5: Mowing environment

Sensing the environment :

Depending on the application, we have to detect :

- a furrow in the ground (Till work)
- a reap limit between mowed and unmowed part (Harvest work)
- a haycock, a strawcock ...(Forage work)

Many sensors has been used :

- video camera
- ultrasonic sensor
- laser telemeter sensor
- mechanical sensor

We have been interested on the reap limit detection by vision to guide :

- a lawn mower
- a combine harvester

2 About the vision aspect

2.1 Introduction

Some applications has been done in agricultural field (not exhaustive) :

- harvesting : Debain in [Deb96], Ollis in [OS96]
- mowing the lawn : Derras in [DBB⁺93] and [DBB91], Debain in [DDB⁺94], Nobutaka in [Nob90],
- collecting tree fruits : Amat in [ABFM93], Sevilla in [SCZD94],
- tomato cultivation : Sandini in [SBMZ90]
- many others ...

In our applications, the aim of the perception part is to detect the reap limit between cut and uncut crop.

Some pictures about cereal

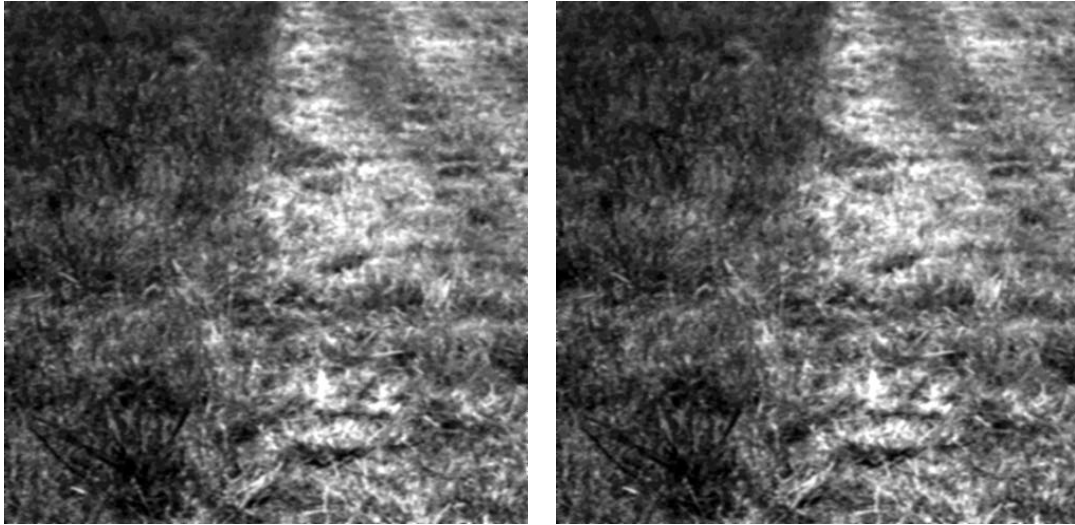


Figure 6: Cereals: weat and oat

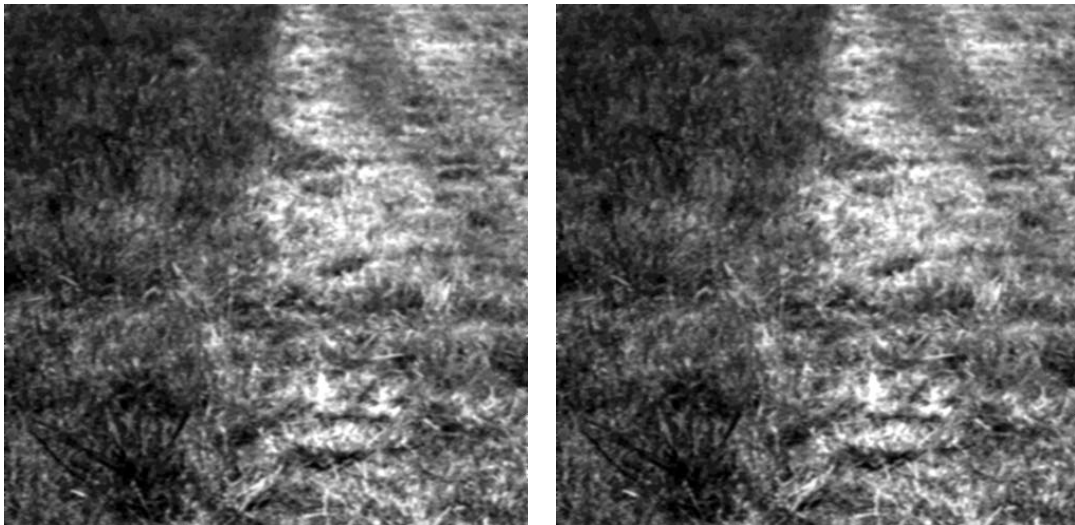


Figure 7: Cereals: corn and sunflowers

2.2 Our Approach

Image Segmentation based on 4 parameters

(*Derras [DBB91]*)

- two parameters of texture (homogeneity, entropy) were chosen using the cooccurrence matrices (texel: region of size 16×16 pixels (*Harlow [HTC86]*)).
- two parameters are computed from local grey-level histograms (the maximum, and the second order of moment of grey-level histograms).

The algorithm:

- unsupervised segmentation method (*Markov field modelling*) (*Genam [GGGD90]*, *Sullins [Sul90]*, *Amat [ABFM93]*).
- extraction of lines candidates for the reape limit
- selection of the line which represents the situation between the vehicle and the reape limit ((θ, ρ) parameters)

For more details of this algorithm: *Derras [DVBB95] [DBB⁺93] [Der93]*.

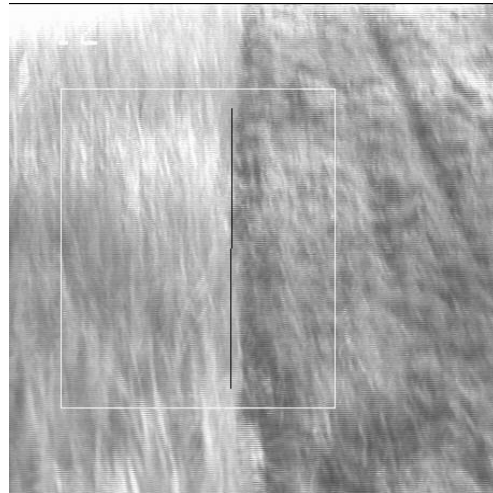
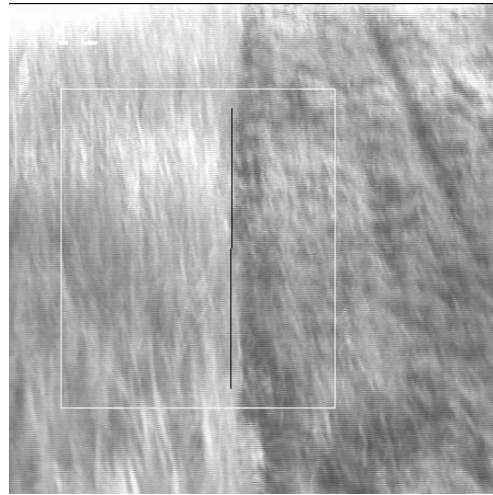
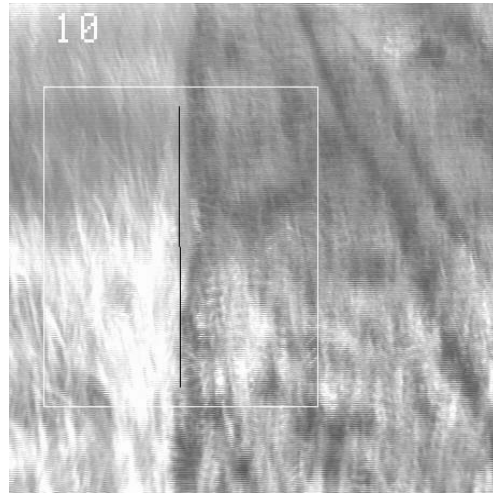


Figure 8: Reap limit detection (*Markov Segmentation*)

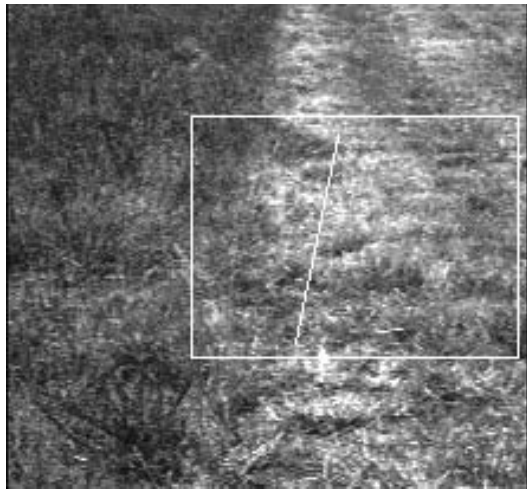


Figure 9: Reap limit estimation

3 AGV in green space environment



Figure 10: Some sample of Machine in green space environment

Figure 11: Mower

Figure 12: The prototype

3.1 Introduction

The application is to guide the lawn mower by vision in regard to cut and uncut limit.

Two main aspects for this application :

- the vision/perception aspect (Derras in [Der93])
- the control aspect (Debain in [Deb96])

The mower is a professional lawn mower built by **Guerin Courde**

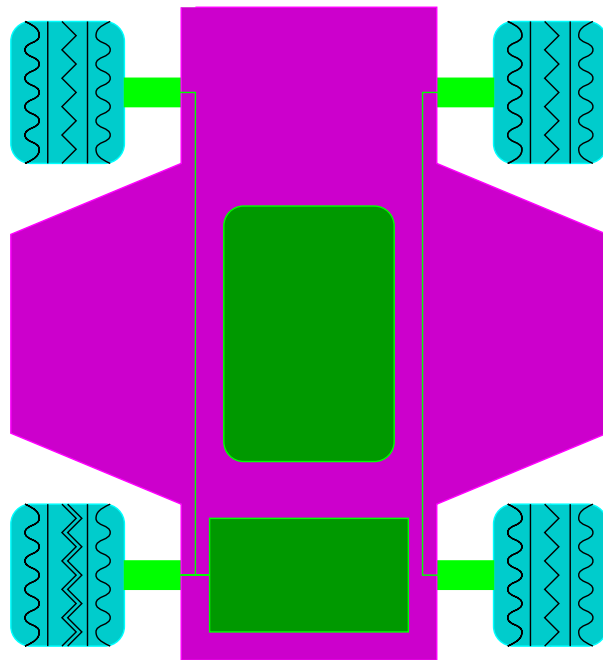


Figure 13: The lawn mower

3.2 Modelling of the Scene

Modelling considerations

To model the scene we use two parameters in image space :

- d represents the distance
- θ represents the orientation

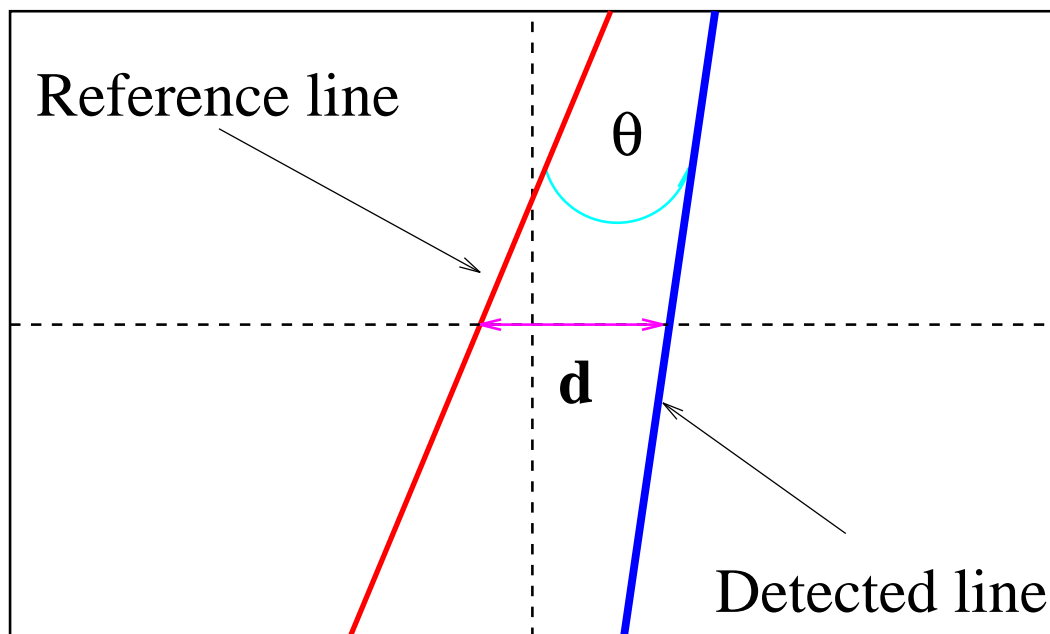


Figure 14: Modelling the scene in image space

Modelling the Mower

We use a machine with :

- four driven wheels.
- the gap is insured the difference $V_2 - V_1$
- non-holonomous

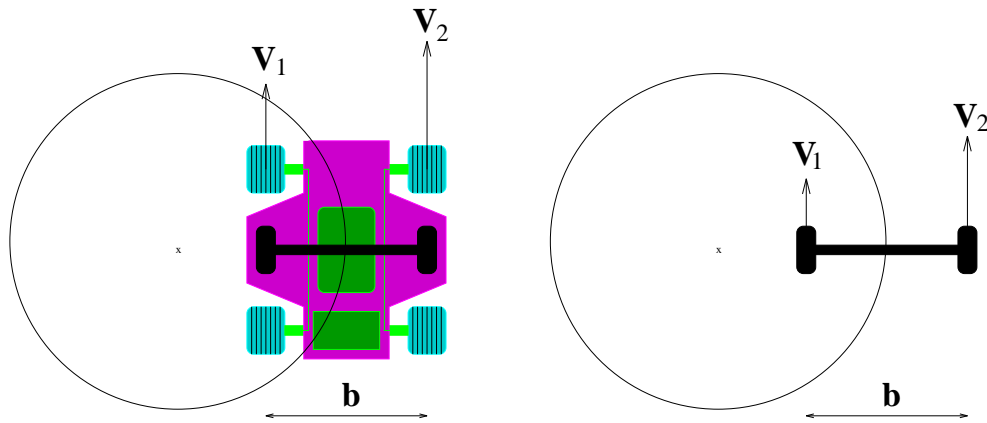


Figure 15: Modelling with a virtual axle

We model the mower with :

- a virtual fixed axle (with 2 wheels).
- each point of this axle move on a circle

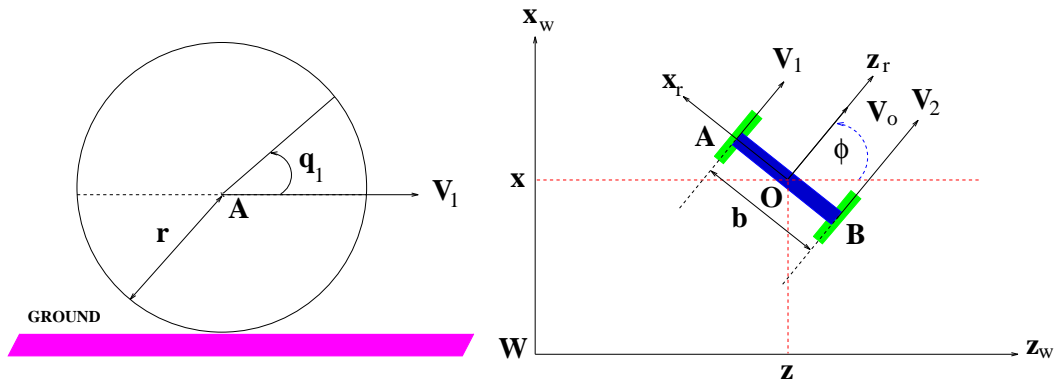


Figure 16: Kinematic modelling

Kinematic equations are :

$$\begin{bmatrix} \dot{x} \\ \dot{z} \\ \dot{\phi} \end{bmatrix} = \begin{pmatrix} \frac{r}{2} \sin \phi & \frac{r}{2} \sin \phi \\ \frac{r}{2} \cos \phi & \frac{r}{2} \cos \phi \\ -\frac{r}{b} & \frac{r}{b} \end{pmatrix} \cdot \begin{bmatrix} \dot{q}_1 \\ \dot{q}_2 \end{bmatrix} \quad (1)$$

We observe :

$$\dot{x} = \dot{z} \cdot \tan \phi \quad (2)$$

We can write :

$$\begin{cases} v = \frac{(V_1 + V_2)}{2} = \frac{r}{2} (\dot{q}_1 + \dot{q}_2) \\ \dot{\phi} = \frac{(V_2 - V_1)}{b} = \frac{r}{b} (\dot{q}_2 - \dot{q}_1) \end{cases} \quad (3)$$

These relations show :

- $v = V_{moy}$ is constant and represents the velocity of the center of the axle
- the trajectory of O depends only of the orientation ϕ

If V_1 and V_2 are constant, O describes a circle with a radius R as :

$$R = \frac{v}{\dot{\phi}} = \frac{b V_2 + V_1}{2 V_2 - V_1} = \frac{b \dot{q}_2 + \dot{q}_1}{2 \dot{q}_2 - \dot{q}_1} \quad (4)$$

It is the same case, for all point attached to the axle.

So, we retain the following relation to characterize the kinematic of the virtual axle :

$$\left\{ \begin{array}{l} v = \frac{r}{2}(\dot{q}_1 + \dot{q}_2) \\ \dot{\phi} = \frac{r}{b}(\dot{q}_2 - \dot{q}_1) \\ R = \frac{b}{2} \frac{\dot{q}_2 + \dot{q}_1}{\dot{q}_2 - \dot{q}_1} \end{array} \right. \quad (5)$$

In our application, the control variables of the mower are :

- $v = \frac{(V_2 + V_1)}{2}$ which represents the average of the speed of both wheels
- $\Delta v = (V_2 - V_1)$ which represents the difference of the speed of both wheels

V_1 and V_2 represents the speed of the center of both wheels.

We have :

$$\begin{bmatrix} \dot{q}_1 \\ \dot{q}_2 \end{bmatrix} = \begin{pmatrix} \frac{1}{r} & -\frac{1}{2r} \\ \frac{1}{r} & \frac{1}{2r} \end{pmatrix} \cdot \begin{bmatrix} v \\ \Delta v \end{bmatrix} \quad (6)$$

So :

$$\begin{bmatrix} v \\ \Delta v \end{bmatrix} = \begin{pmatrix} \frac{r}{2} & \frac{r}{2} \\ -r & r \end{pmatrix} \cdot \begin{bmatrix} \dot{q}_1 \\ \dot{q}_2 \end{bmatrix} \quad (7)$$

3.3 Trajectory generation

We consider two positions characterized by :

- (dx, dy) the difference in position
- θ the difference in orientation

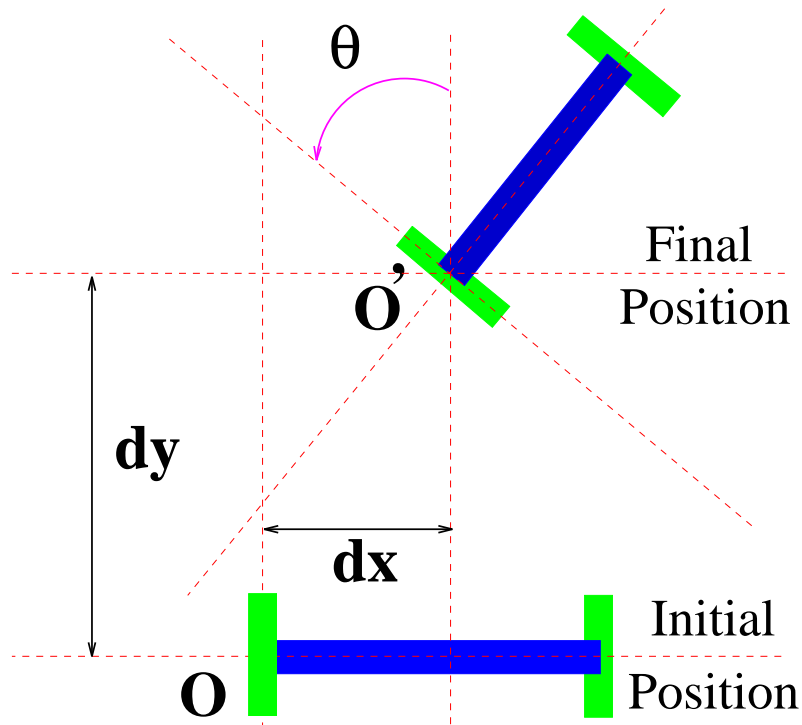
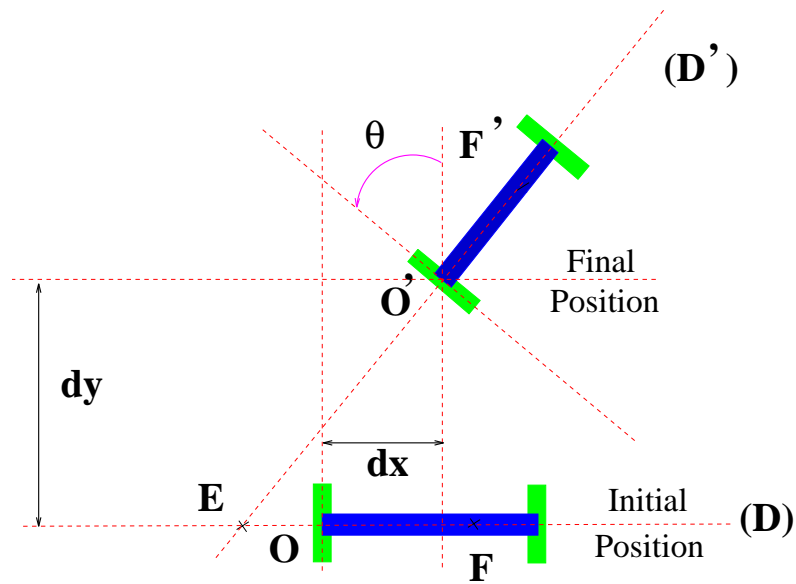


Figure 17: Initial and final position

To control the machine we generate a trajectory composed with 2 circles (as Kelly has done in [KGL91])



We define F on the line (D) with : $OF = \frac{1}{2} \cdot O'F'$

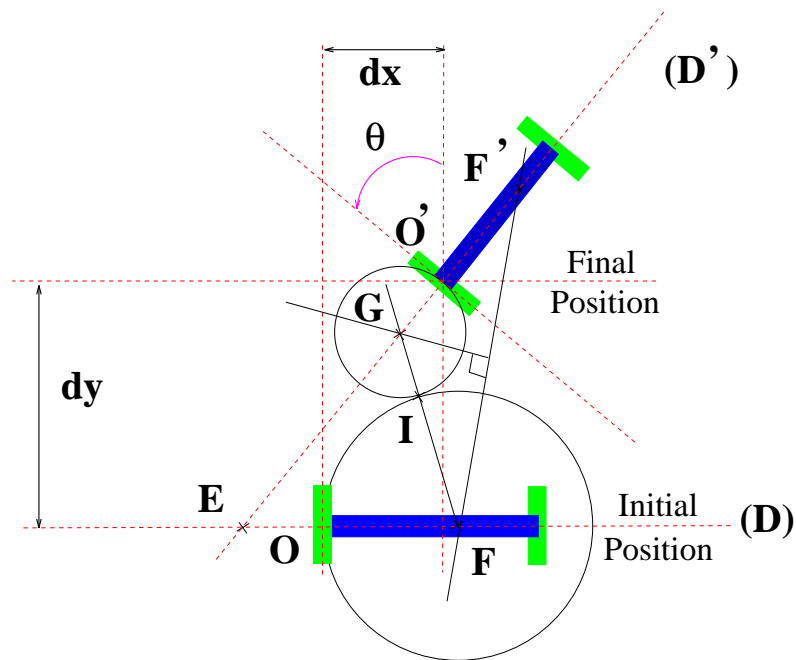


Figure 18: Trajectory generation

The main relation used to defined the trajectory are the following :

The equation of the line (D') is :

$$Y = X.tan\theta + dy - dx.tan\theta \quad (8)$$

The point $E = \left(\frac{dx.tan\theta - dy}{tan\theta}, 0\right)^T$ if $tan\theta \neq 0$

and $F = \left(\frac{-dx + \sqrt{4.dx^2 + 3.dy^2}}{3}, 0\right)^T$

F' is defined as : $OF = O'F' = (X_{f'}, Y_{f'})^T$

So, we have :

$$(X_{f'} - dx)^2 + (Y_{f'} - dy)^2 = OF^2 = dF^2 \quad (9)$$

$$\left\{ \begin{array}{l} Y_{f'} = a.X_{f'} + b \\ X_{f'} = \frac{dx - a.b + a.dy}{1+a^2} \\ \pm \frac{\sqrt{(dx - a.b + dy)^2 - (1+a^2)(dx^2 + (b - dy)^2 - dF^2)}}{1+a^2} \end{array} \right. \quad (10)$$

with $a = tan\theta$ and $b = dy - dx.tan\theta$

G is defined as :

$GF = R_1 + R_2$ and $GF = GF'$

Knowing the two angle and radius of the circle, we can determine the velocities to apply on the lawn mower.

We have shown that :

$$R = \frac{b \dot{q}_2 + \dot{q}_1}{2 \dot{q}_2 - \dot{q}_1} \quad (11)$$

In our applications, $v = V_{moy} = \frac{r}{2}(\dot{q}_2 + \dot{q}_1) = cste$, then we obtain :

$$\begin{cases} \dot{q}_1 = \frac{V_{moy}}{2.R.r}(2.R - b) \\ \dot{q}_2 = \frac{V_{moy}}{2.R.r}(2.R + b) \end{cases} \quad (12)$$

Using relation 7, we deduce :

$$\begin{cases} v = V_{moy} \\ \Delta v = \frac{b.V_{moy}}{R} \end{cases} \quad (13)$$

So, knowing the initial and final position, we decompose the trajectory with two circles and deduce the radius of curvature for both.

Remark :

As shown in the next figures, we can adapt the trajectory in function of the type of error :

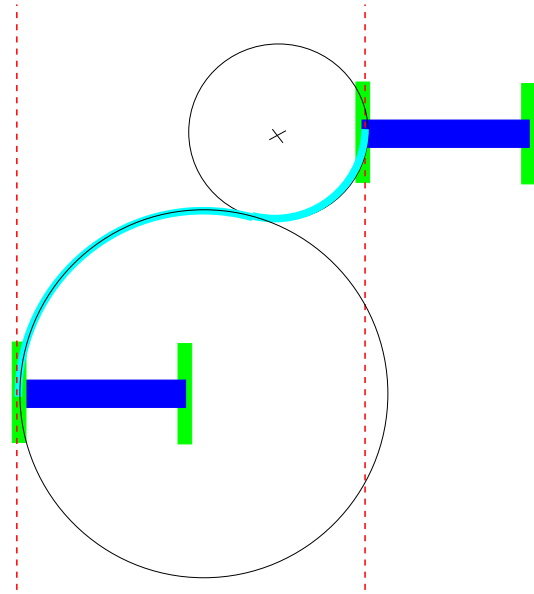


Figure 19: Lateral error

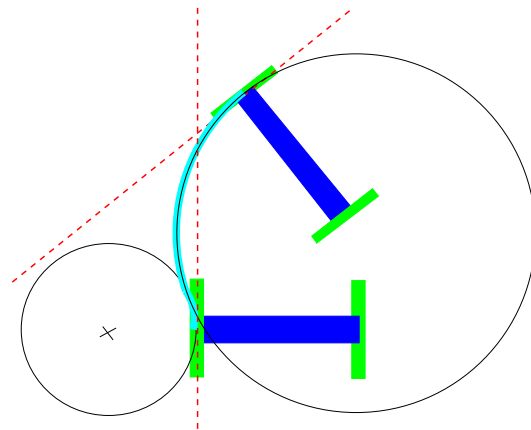


Figure 20: Orientation error

3.4 Results

Simulation Results :

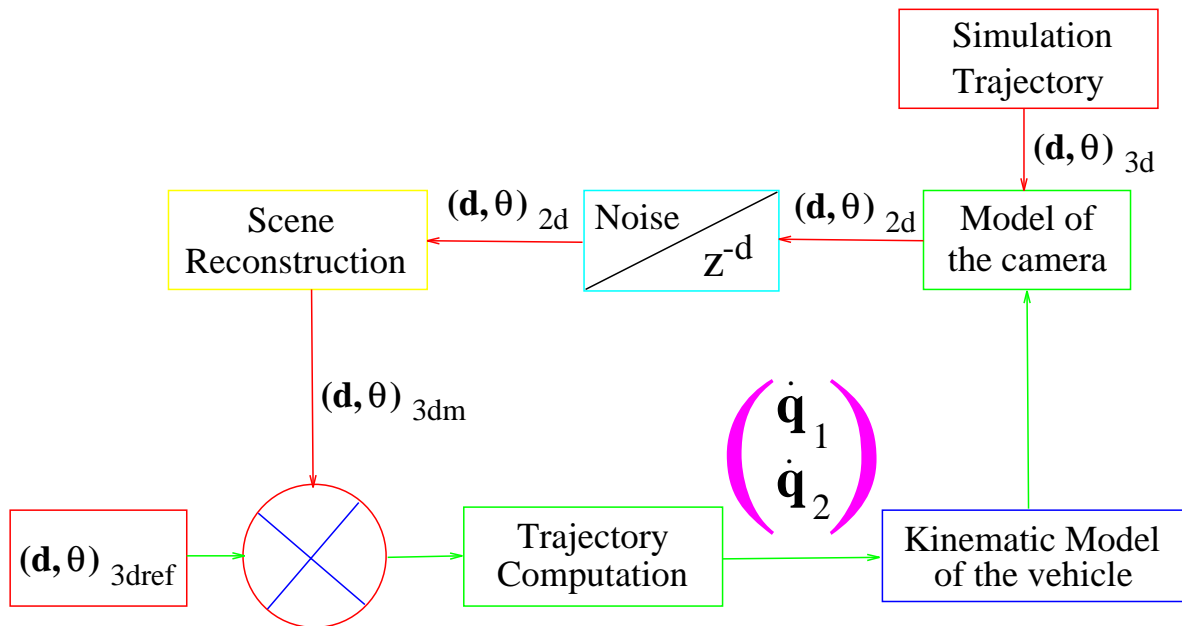
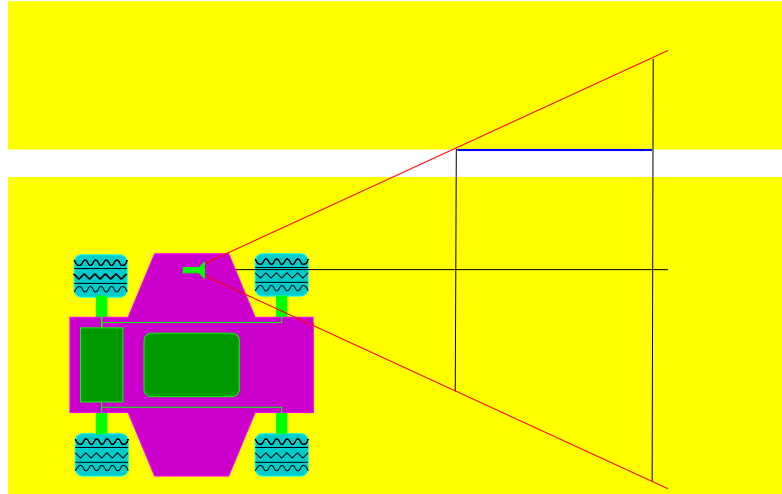


Figure 21: Functionalities of the simulator

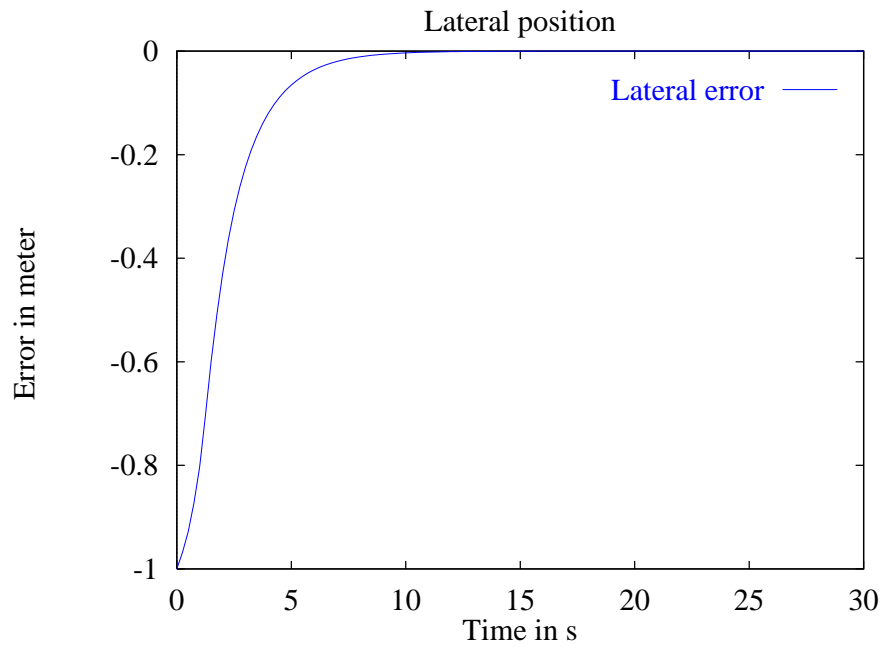


Figure 22: Lateral position of the mower

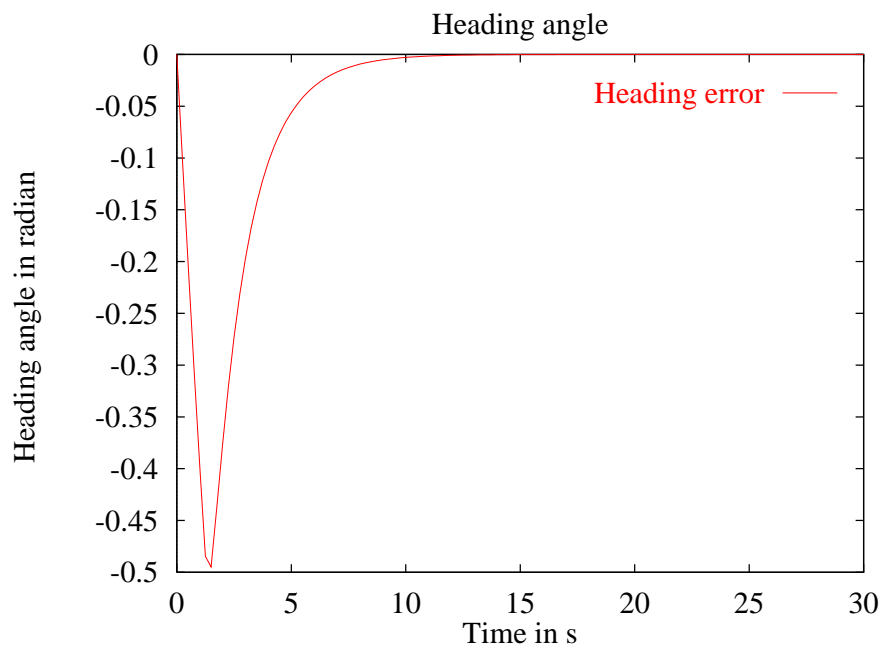


Figure 23: Orientation of the mower

Simulation Results with noise:

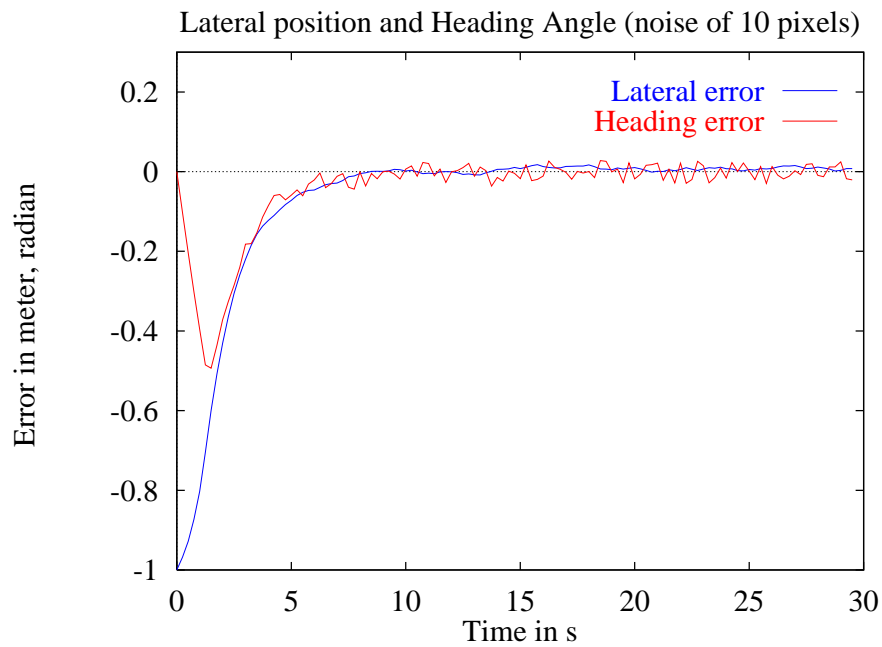


Figure 24: Position and Orientation with noise (10 pixels)

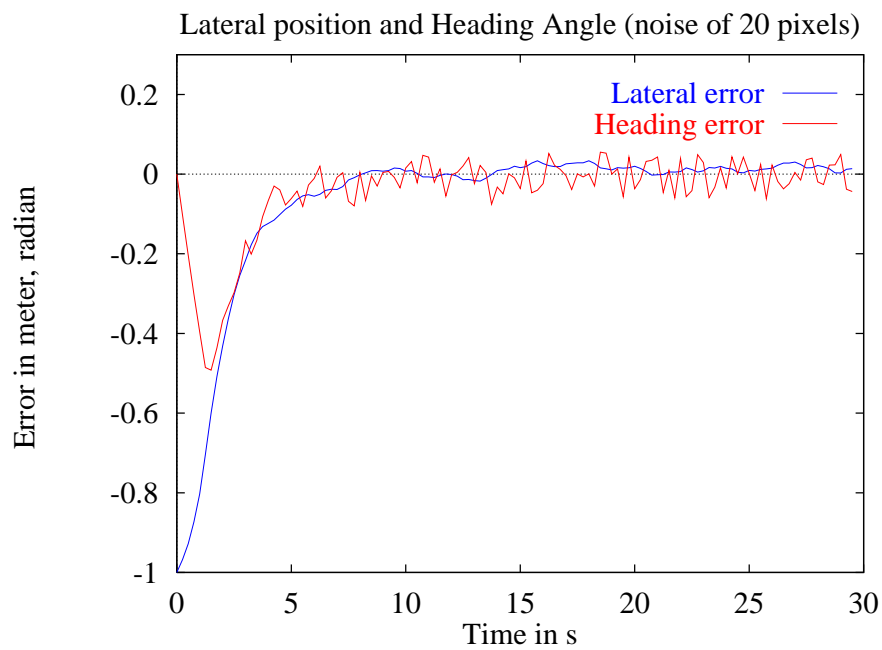


Figure 25: Position and Orientation with noise (20 pixels)

Experimental Results :

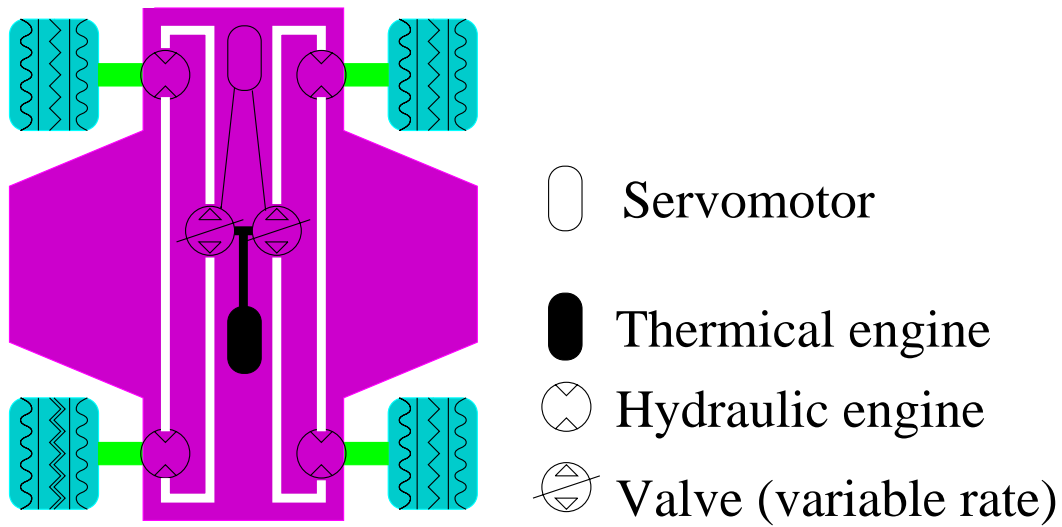


Figure 26: Hydraulic actuators

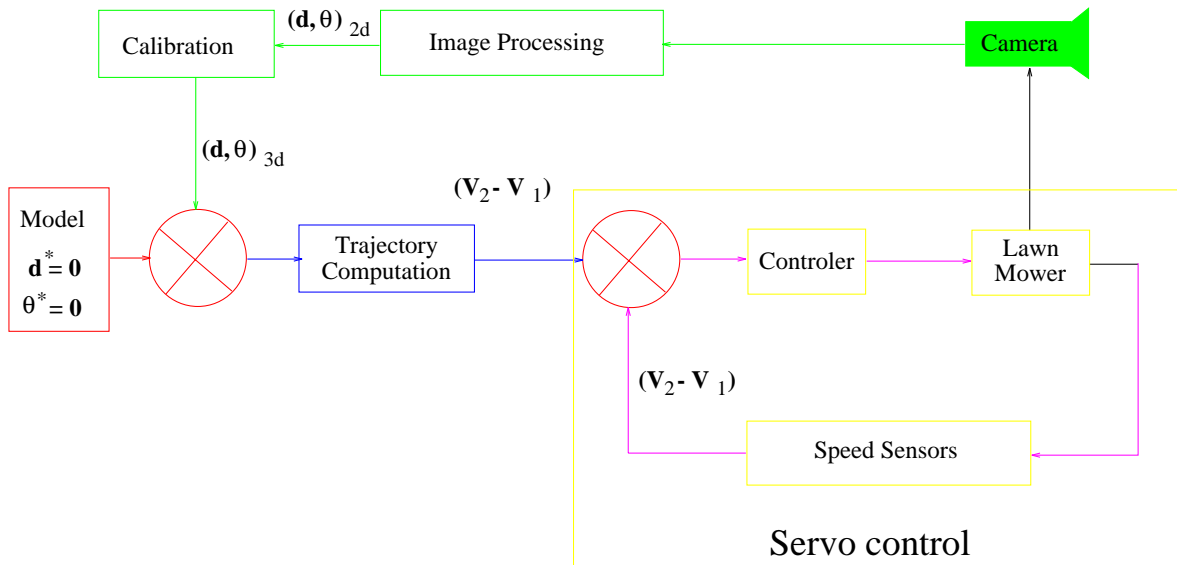


Figure 27: Visual servoing scheme (servo control)

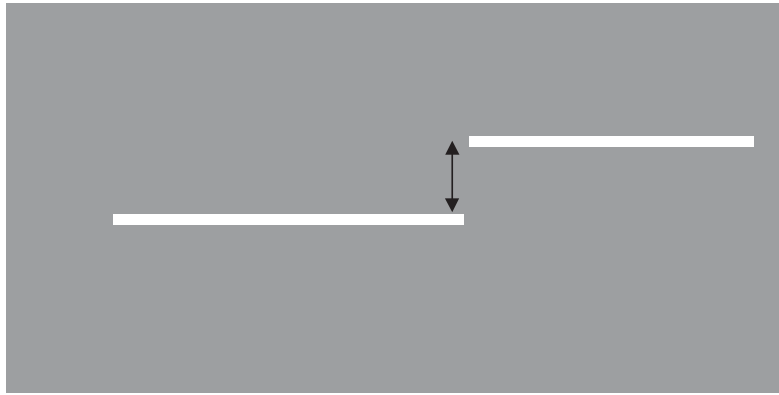


Figure 28: Experimental conditions (step of 50 cm)

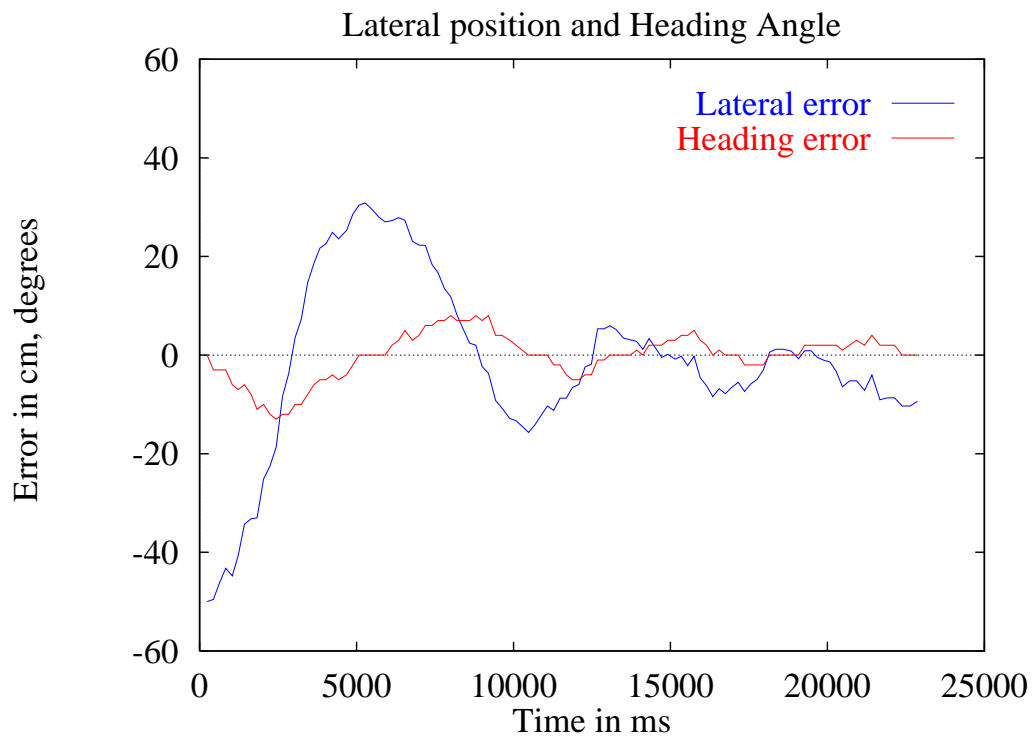


Figure 29: Position and Orientation of the mower

4 AGV in agricultural field

4.1 Introduction

Application context: Harvesting

- use of a combine harvester
- use of vision sensor
- help the driver in vehicle guidance

Vision aspect:

- similar to those encountered in green space environment
- use of the same algorithm

Control aspect:

- controller design in the sensor space
- evaluation of different control laws
- vehicle guidance on a slope ground (first results)



Figure 30: CLASS and CASE



Figure 31: AGCO (*Massey Ferguson & Gleaner*)



Figure 32: FORD NEW HOLLAND



Figure 33: CLASS : *dreschs and le480s*



Figure 34: CLASS: *Cab and Control*

Figure 35: CLASS: *Our combine harvester*

4.2 Modelling of the Scene

Modelling considerations (*Chaumette [Cha90], Hager [HHC96]*)

- interaction matrix or image jacobian
- classical *pinhole* approximation of the camera
- T_c represents the camera velocity screw
- \underline{s} represents the visual informations

We can write :

$$\dot{\underline{s}} = L_{\underline{s}}^T T_c \quad (14)$$

where $L_{\underline{s}}^T$ is the interaction matrix related to \underline{s} .

The interaction matrix $L_{\underline{s}}^T$:

- depends on the nature of the visual information contained in \underline{s}
- is obtained by using the well known equation of optical flow measurement to 3D structure and motion in the scene (*Faugeras [Fau93], Paul [Pau82]*).

Modelling the scene

The scene is represented by a straight line and modelled by its projected line in the image frame.

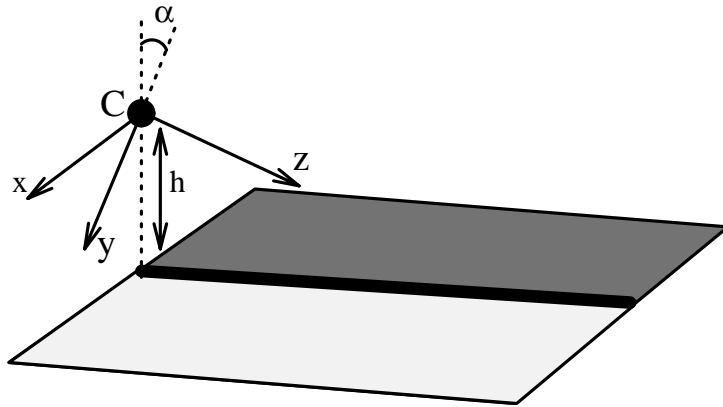


Figure 36: 3D camera frame

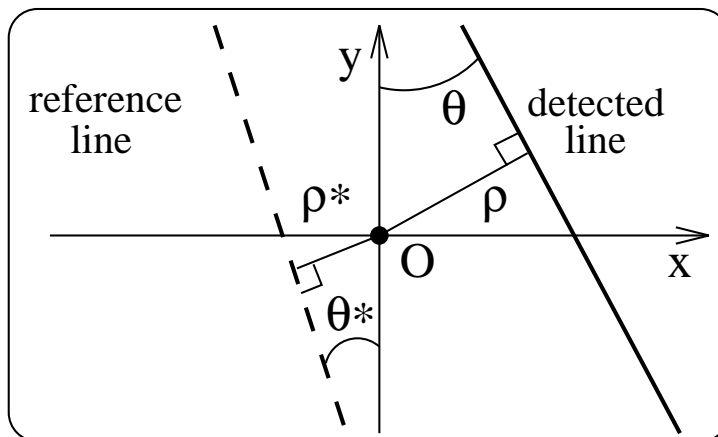


Figure 37: 2D camera frame

The position of the machine and its orientation is expressed according to the set of visual features :

$$\underline{s} = (\theta, \rho)^T \quad (15)$$

At the equilibrium situation , $\underline{s} = \underline{s}^*$, we have :

$$\underline{\dot{s}} = L_{|\underline{s}=\underline{s}^*}^T T_c \quad (16)$$

The equation of the plane containing the desired line is expressed as :

$$y \cos \alpha - z \sin \alpha + h = 0 \quad (17)$$

where α represents the angle of inclination of the camera.

Considering expression (14), at the equilibrium situation, the interaction matrix $L_{\underline{s}}^T$ becomes :

$$L_{|\underline{s}=\underline{s}^*}^T = \begin{pmatrix} \lambda_{\theta}^* \cos \theta^* & \lambda_{\theta}^* \sin \theta^* & -\lambda_{\theta}^* \rho^* \\ \lambda_{\rho}^* \cos \theta^* & \lambda_{\rho}^* \sin \theta^* & -\lambda_{\rho}^* \rho^* \\ -\rho^* \cos \theta^* & -\rho^* \sin \theta^* & -1 \\ (1 + \rho^{*2}) \sin \theta^* & -(1 + \rho^{*2}) \cos \theta^* & 0 \end{pmatrix}$$

with :

$$\begin{cases} \lambda_{\theta}^* & = & -(\cos \alpha \cos \theta^*)/h \\ \lambda_{\rho}^* & = & (\rho^* \cos \alpha \sin \theta^* - \sin \alpha)/h \end{cases}$$

4.3 Control Aspect

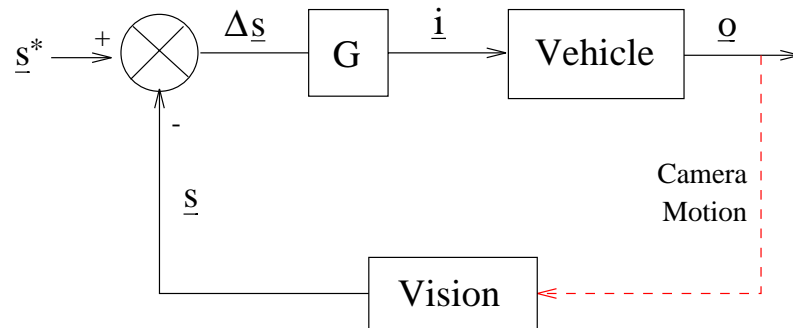


Figure 38: Servoing scheme

- \underline{s}^* = a reference target image,
- \underline{s} = the current visual information ,
- G = the vector control gain,
- \underline{i} = the control variable of the machine (steering angle of the machine),
- \underline{o} = a set of outputs characterizing the machine's position and orientation.

Two kinds of control law will be presented :

- task function approaches
- neural network approach.

4.3.1 Task Function Approach

The **task function** approach was developed by *Espiau, Samson et al* ([*ECR92*], [*SBE91*]).

This function can be thought of as representing a **virtual kinematic** constraint between the camera and the target. In this case, we explicitly use the **modelling of the vehicle** in order to synthesize the **control law**.

(a) Vehicle Modelling

We use a machine with :

- two steerable wheels,
- two driven wheels.

At a constant steering angle, this machine describes a circle. The model of the vehicle assumes the following :

- there are no flexible parts,
- the vehicle moves on plane surface,
- there is no translational slip between the wheels and the surface,
- there is sufficient rotational friction between the wheels and the surface.

We consider the steering mechanism as the same as a bicycle.

- the two rear wheels turn slightly differentially
- the instantaneous centre of rotation can be determined purely by kinematic means

Let $\dot{\psi}$ the angular velocity vector directed along the y axis, and \dot{x} the linear velocity directed along x axis.

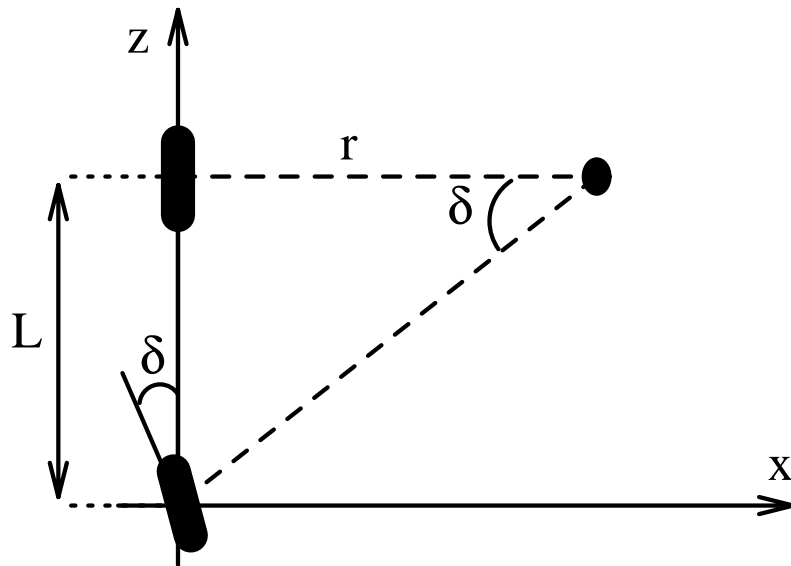


Figure 39: Bicycle model

Using the bicycle model approximation (see Figure 39), the steering angle δ and the radius of curvature r are related to the wheelbase L , as in (Kelly [Kel94]) by:

$$\tan \delta = -\frac{L}{r} \quad (18)$$

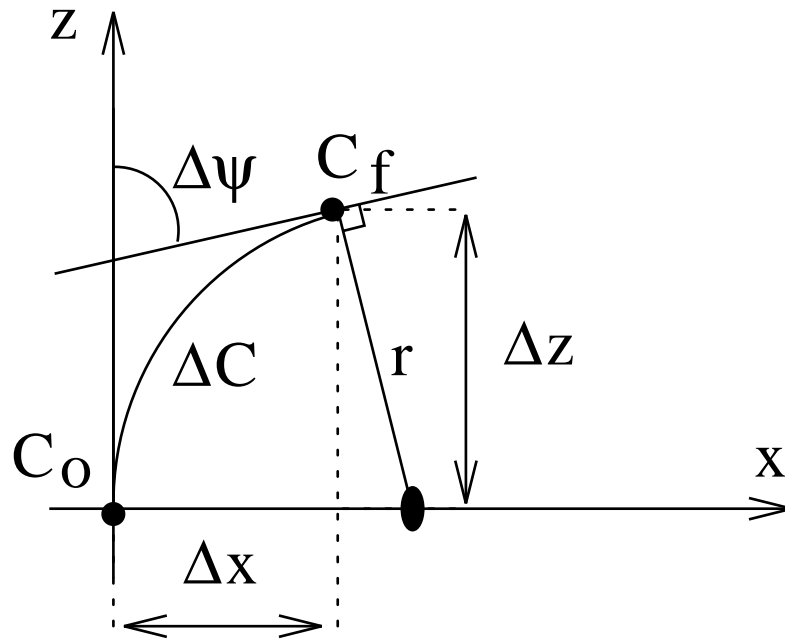


Figure 40: Vehicle trajectory

In Figure 40 we show a small portion of a circle ΔC representing the trajectory to be followed by the machine. We assume that it moves with small displacements between an initial curvilinear abscissa C_0 and a final one named C_f such that:

$$\begin{cases} \frac{1}{r} = \lim_{\Delta C \rightarrow 0} \frac{\Delta \psi}{\Delta C} = \frac{d\psi}{dC} = \dot{\psi} \\ \dot{C}^2 = \dot{x}^2 + \dot{z}^2 \end{cases} \quad (19)$$

In fact, the rotational velocity is obtained as:

$$\dot{\psi} = -\frac{\tan \delta}{L} \sqrt{\dot{x}^2 + \dot{z}^2} \quad (20)$$

The lateral position denoted by x can be computed by assuming that the machine moves with small displacements. In the case of longitudinal motion along the z axis during a time interval Δt , we express:

$$\begin{cases} \Delta z = r \sin \Delta \psi \\ \Delta x = r(1 - \cos \Delta \psi) \end{cases} \quad (21)$$

Eliminating r from equations (21), we obtain:

$$\Delta x = \Delta z \frac{1 - \cos \Delta \psi}{\sin \Delta \psi} \quad (22)$$

Without loss of generality, we can consider that the initial conditions are null since the frame is linked at the position C_0 and then $\Delta x = x$, $\Delta z = z$ and $\Delta \psi = \psi$. We compute the derivative over time of the lateral coordinate x of the machine given by (22) which depends on z and ψ , as follows:

$$\dot{x} = \frac{1 - \cos \psi}{\sin \psi} \left[\dot{z} + \frac{z \dot{\psi}}{\sin \psi} \right] \quad (23)$$

Using the approximation to small angles (ψ and δ are less than 7°) and considering that the machine moves with constant longitudinal speed $\dot{z} = V$ and that $\dot{x} \ll V$, we can write:

$$\dot{x} = \frac{\psi}{2} \left(\dot{z} + \frac{z}{\psi} \dot{\psi} \right) \quad (24)$$

Taking into account the approximations below, we have $\dot{\psi} \approx \frac{\dot{z}}{r}$ and $\psi \approx \frac{z}{r}$ since the r is supposed to be constant.

We finally find the kinematic model of the machine expressed by the following equations which are similar to those obtained by another method (*Khadraoui [KMG95]*):

$$\begin{cases} \dot{\psi} = -\frac{V}{L}\delta \\ \dot{x} = V\psi \end{cases} \quad (25)$$

However, we only control the wheel angle δ . We can find an equation linking δ to the vector $(V, \dot{\psi})$.

In our application, we consider that the velocity V is constant, then we have (*Murray [MS93], Ioos [IBT88]*) :

$$\delta = -\frac{L}{V}\dot{\psi}$$

(b) State Space Controller Design

We treat here a single input linear system with output parameters (θ, ρ) .

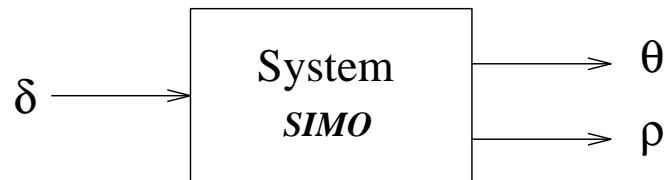


Figure 41: Considered system

We search a state model which integrates both the model of the machine and that of the scene.

The mobile robot moves with limited degrees of freedom. It has non-holonomic constraints since the number of degrees of freedom of control, δ in our case, is less than the number of degrees of freedom of displacement : translation along x and z axes and rotation around the y axis.

In the case where the desired situation is represented by a straight line centered in the image ($\theta^* = \rho^* = 0$) and by considering equation (16), we can express the kinematic screw T_c as :

$$T_c = L_{|\underline{s}=\underline{s}^*}^{T+} \dot{\underline{s}} \quad (26)$$

Determination of the kernel of the interaction matrix (matrix of rank 2), permits us to constrain the lateral translation of the vehicle and its orientation by introducing a rank 2 matrix such as:

$$T_c = \begin{bmatrix} 1 & 0 & 0 & 0 & 0 & 0 \\ 0 & 0 & 0 & 0 & 1 & 0 \end{bmatrix} L_{|\underline{s}=\underline{s}^*}^{T+} \dot{\underline{s}} \quad (27)$$

Consequently, the matrix $L_{|\underline{s}=\underline{s}^*}^{T+}$ is limited to the components that correspond to the lateral and the orientation movements :

$$\dot{\underline{s}} = \begin{bmatrix} l_{11} & l_{12} \\ l_{21} & l_{22} \end{bmatrix} \begin{pmatrix} V_x \\ \Omega_y \end{pmatrix} \quad (28)$$

with

$$\begin{cases} l_{11} & = & \lambda_{\theta}^* \cos \theta^* \\ l_{12} & = & -\rho^* \sin \theta^* \\ l_{21} & = & \lambda_{\rho}^* \cos \theta^* \\ l_{22} & = & -(1 + \rho^{*2}) \cos \theta^* \end{cases}$$

We remark that the velocities V_x and Ω_y correspond to those expressed in (25) for the machine. We write:

$$\begin{cases} V_x = \dot{x} & = & V\psi \\ \Omega_y = \dot{\psi} & = & -\frac{V}{L}\delta \end{cases} \quad (29)$$

and

$$\begin{pmatrix} \dot{x} \\ \dot{\psi} \end{pmatrix} = \begin{bmatrix} l_{11} & l_{12} \\ l_{21} & l_{22} \end{bmatrix}^{-1} \begin{pmatrix} \dot{\theta} \\ \dot{\rho} \end{pmatrix} \quad (30)$$

By integrating (30) over time we have:

$$\begin{pmatrix} x \\ \psi \end{pmatrix} = \frac{1}{\Delta l} \begin{bmatrix} l_{22} & -l_{12} \\ -l_{21} & l_{11} \end{bmatrix} \begin{pmatrix} \theta \\ \rho \end{pmatrix} + \begin{bmatrix} k_1 \\ k_2 \end{bmatrix} \quad (31)$$

with:

$$\Delta l = l_{11}l_{22} - l_{21}l_{12}$$

Using (29) and (31), we can easily express the velocities V_x and Ω_y :

$$\begin{cases} V_x & = & \frac{V}{\Delta l}(-l_{21}\theta + l_{11}\rho) + k_2V \\ \Omega_y & = & -\frac{V}{L}\delta \end{cases} \quad (32)$$

By considering equations (28) and (32), and developing, the state representation of the system with initial conditions null ($k_2 = 0$ if $\theta^* = 0$ and $\rho^* = 0$) is given by :

$$\begin{pmatrix} \dot{\theta} \\ \dot{\rho} \end{pmatrix} = \frac{V}{\Delta l} \begin{bmatrix} -l_{11}l_{21} & l_{11}^2 \\ -l_{21}^2 & l_{11}l_{21} \end{bmatrix} \begin{pmatrix} \theta \\ \rho \end{pmatrix} - \frac{V}{L} \begin{bmatrix} l_{12} \\ l_{21} \end{bmatrix} \delta \quad (33)$$

The state-space form of the model becomes:

$$\underline{\dot{s}} = A \underline{s} + B \delta \quad (34)$$

where:

- \underline{s} = the current visual information vector,
- δ = the control variable,
- A and B are constant matrices.

The control law is synthesized using a pole assignment technique (second order system having ξ as a damping ratio and ω_0 as its frequency). Finally, the gain matrix is expressed as follows:

$$G = (g_1 \ g_2) \quad (35)$$

with :

$$\begin{cases} g_1 = \frac{L \omega_0}{V^2 \Delta l} (2 V \xi l_{21} - \omega_0 l_{22}) \\ g_2 = -\frac{L \omega_0}{V^2 \Delta l} (2 V \xi l_{11} - \omega_0 l_{12}) \end{cases} \quad (36)$$

(c) Regulation of two Task Functions

We define a global task function \underline{e} such as :

$$\underline{e} = C(\underline{s} - \underline{s}^*) \quad (37)$$

where

- \underline{e} is a six dimensional vector (6x1),
- $\underline{s} - \underline{s}^*$ is a vector of two components (2x1),
- C is the combination matrix (6x2).

The visual information used in our application is as shown in Figure 42:

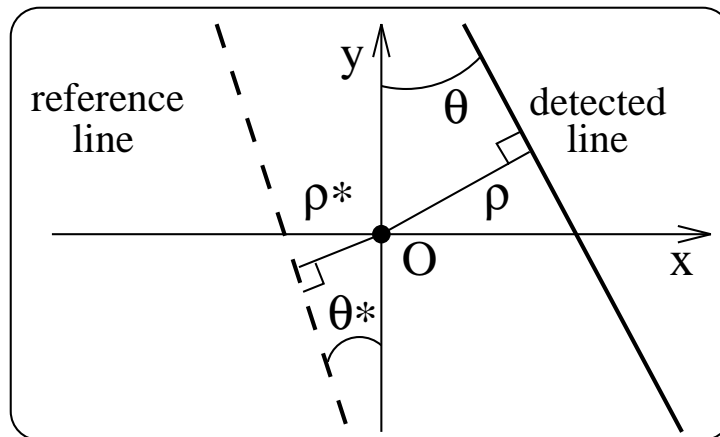


Figure 42: Image space

We can write:

$$C = (C_1, C_2) \quad (38)$$

From equation (37), we have :

$$\underline{e} = C_1(\theta - \theta^*) + C_2(\rho - \rho^*) = \underline{e}_\theta + \underline{e}_\rho \quad (39)$$

In the case where the object stays fixed on the camera frame, a possible proportional control law is :

$$T_c = -\lambda \underline{e} \quad (40)$$

We choose a similar control law given by :

$$T_c = -\lambda(\beta \underline{e}_\theta + \underline{e}_\rho) \quad (41)$$

λ and β two non-zero positive real values.

This amounts to introducing a supplementary gain on one part of the error, the one concerning the heading error. In fact, the different types of drive of a mobile robot mean that we can give different degrees of importance to the lateral error and the heading error.

A precise but abrupt drive requires a lot of energy, favouring lateral error, whereas a smooth, non-precise drive emphasizes heading error.

Consequently, we first impose an exponential decay on \underline{e}_θ and another on \underline{e}_ρ by writing:

$$\underline{\dot{e}} = -\lambda(\beta\underline{e}_\theta + \underline{e}_\rho) \quad (42)$$

By using the classical methods of the form of vision-based control, we can calculate the control matrix. We differentiate the equation (39) as follows :

$$\underline{\dot{e}} = C\underline{\dot{s}} = C_1\dot{\theta} + C_2\dot{\rho} \quad (43)$$

where λ and β are scalar and are in R^{*+} and with (42), we obtain :

$$\underline{\dot{e}} = -\lambda C \begin{pmatrix} \beta & 0 \\ 0 & 1 \end{pmatrix} \begin{pmatrix} \theta - \theta^* \\ \rho - \rho^* \end{pmatrix} \quad (44)$$

Finally, (43) and (44) give :

$$C\underline{\dot{s}} = -\lambda CB(\underline{s} - \underline{s}^*) \quad (45)$$

with

$$B = \begin{pmatrix} \beta & 0 \\ 0 & 1 \end{pmatrix}$$

As is given in [CRE91], a possible value of C in order to satisfy the conditions of convergence near the desired position is

$$C = L_{(\underline{s}=\underline{s}^*)}^{T+} \quad (46)$$

Here, L^{T+} is the pseudo-inverse of the interaction screw calculated for the equilibrium position $\underline{s} = \underline{s}^*$.

Near the the equilibrium position, the modelling of the scene gives us the following :

$$\dot{\underline{s}} = L_{(\underline{s}=\underline{s}^*)}^T T_c \quad (47)$$

T_c is the kinematic screw represented by six degrees of freedom of the camera. We can deduce from equations (45), (46) and (47) :

$$T_c = -\lambda L_{(\underline{s}=\underline{s}^*)}^{T+} B(\underline{s} - \underline{s}^*) \quad (48)$$

T_c gives us a velocity control of our camera and having the expression of Ω_y we deduce the value of the control input of our system expressed in the modelling of the vehicle (eqn. 4.3.1). It is given by :

$$\delta = -\frac{\lambda L}{V} \left[\beta \frac{\sin \alpha \cos \alpha}{1+h^2} (\theta - \theta^*) - \frac{h^2 + \cos^2 \alpha}{1+h^2} (\rho - \rho^*) \right] \quad (49)$$

4.3.2 Neural Approach

(a) Introduction to the Neural Network

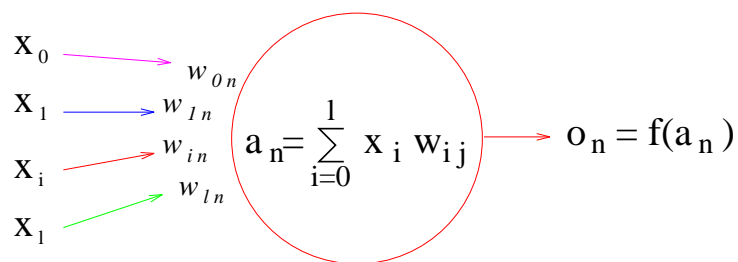


Figure 43: Cell of a neural network

(a-1) Neural network with one hidden level

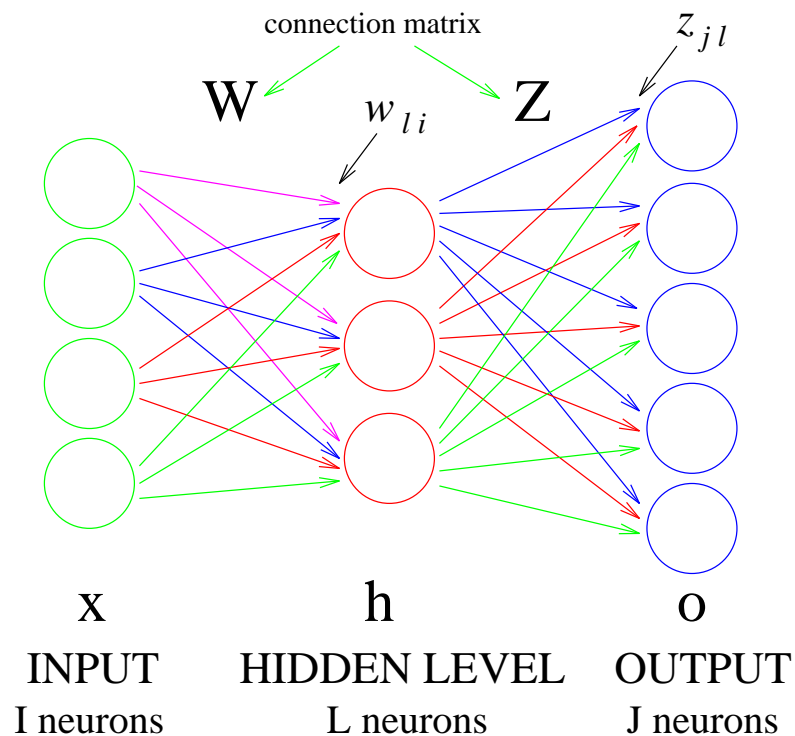


Figure 44: Neural network with one hidden level

(a-2) The back-propagation algorithm

Notations:

- x_k k^{eme} stimulus vector (dim. I),
- h_k k^{eme} output vector of the hidden level (dim. L),
- o_k k^{eme} output vector of neural network (dim. J),
- t_k k^{eme} desired output vector (dim. J),
- e_k k^{eme} error vector (dim. J),
- W connection matrix between input and hidden level (dim. LxI),
- Z connection matrix between hidden and output level (dim. JxL),
- f transfert function (i.e : $f(x) = \frac{1}{1+e^{-x}}$)

We have :

$$\begin{cases} o_k = f(Z.h_k) \\ h_k = f(W.x_k) \\ e_k = (t_k - o_k) \end{cases} \quad (50)$$

(a-3) The back-propagation algorithm (next)

We define the output error signal as:

$$\delta_{out,k} = f'(Z.h_k) \odot (e_k) = o_k \odot (1 - o_k) \odot (t_k - o_k) \quad (51)$$

(\odot represents the Hadamar product)

At the step $t + 1$, $Z_{[t]}$ becomes :

$$Z_{[t+1]} = Z_{[t]} + \eta \delta_{out,k} . h_k^T = Z_{[t]} + \Delta_{[t]} Z \quad (52)$$

with η a positive real number

For the hidden level, the error signal is back-propagated:

$$\delta_{hid,k} = f'(W.x_k) \odot (Z_{[t]}^T . \delta_{out,k}) = h_k \odot (1 - h_k) \odot (Z_{[t]}^T . \delta_{out,k}) \quad (53)$$

At the step $t + 1$, $W_{[t]}$ becomes :

$$W_{[t+1]} = W_{[t]} + \eta \delta_{hid,k} . x_k^T = W_{[t]} + \Delta_{[t]} W \quad (54)$$

with η a positive real number

This algorithm minimize the square of the error a each step. This procedure corresponds to the minimum research of a function using the gradient technique.

(b) Application in agricultural field

(b-1) Neural Model

Using the lateral ρ_i and heading θ_i errors defined in the image reference, the steering controller has to compute steering commands to obtain the minimum difference between the vehicle and the line followed.

We chose a multilayer neural network because it has been used successfully in multiple areas such as classification, modelling and automation (*LeCun [Le 87]*).

The learning algorithm is the classical gradient method which aims at reducing the following error function (*Abbassi [AS91], Rumelhart [Ra86]*) :

$$E_{rr} = \sum_{k=1}^n E^k \quad (55)$$

with

$$E^k = \sum_1^m (\delta d_i^k - \delta r_i^k)^2$$

and

- n the number of sample,
- m the number of outputs,
- δd_i^k the expected output,
- δr_i^k the real output.

(b-2) Neural Network architecture

For the choice of the size on the network, the risk is double edged:

- a smaller number of neurons leads to insufficient modelling.
- too many neurons leads to excessive modelling which can reduce the performance of the network.

The final choice of network (see figure 45) has:

- two inputs (heading and lateral position of the line detected in the image)
- one output (the steering angle)
- two hidden levels (two neurons, five neurons)

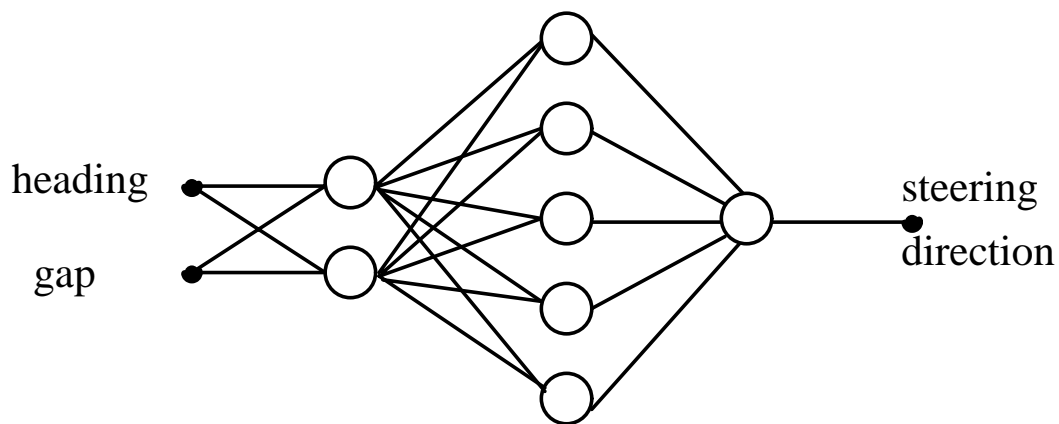


Figure 45: Choice of neural network architecture

(b-3) Training the Network

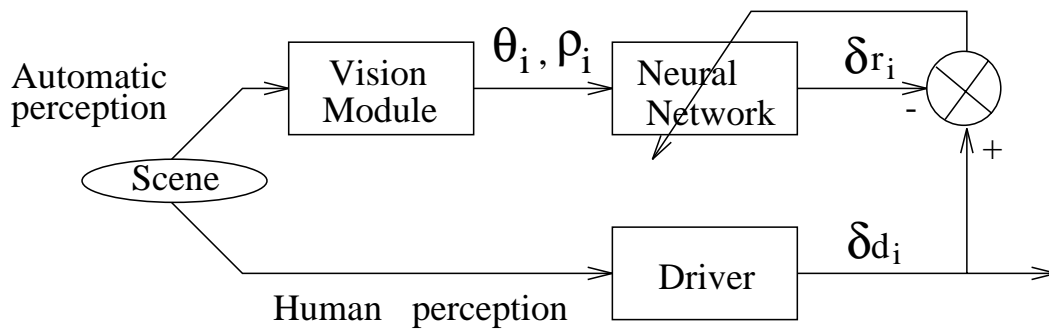


Figure 46: Principle of neural network learning

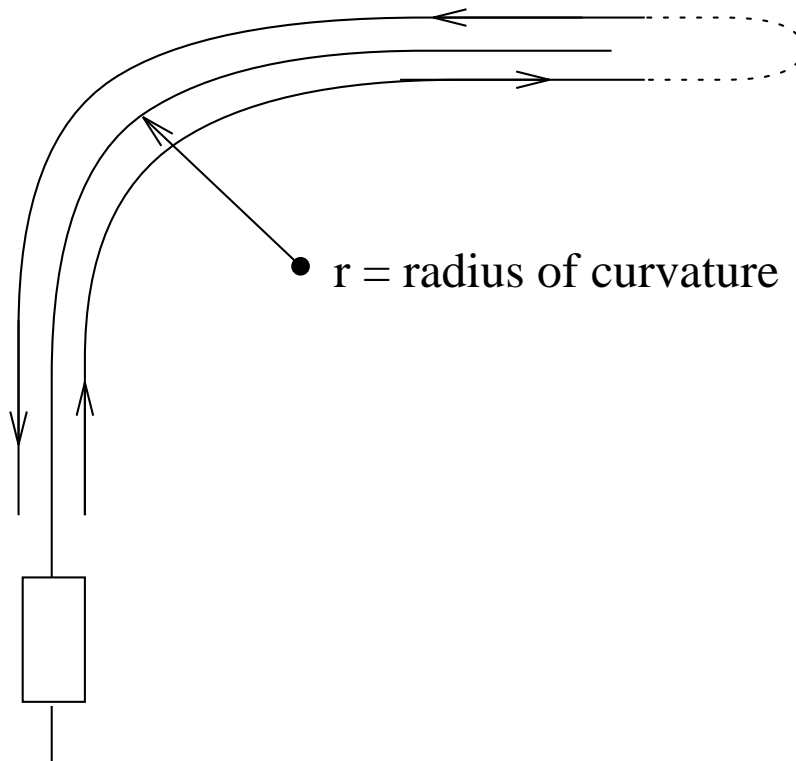


Figure 47: Creation of learning data

The sets of datas $(\rho_i, \theta_i, \delta d_i)$ are available at a regular rate. With the sampled data, the back-propagation algorithm used in the gradient method can lead to local minima (*Dayhoff [Day90], McInerney [IHBHN89]*). In order to avoid them, the learning step is divided into two parts (Figure 48 and 49) :

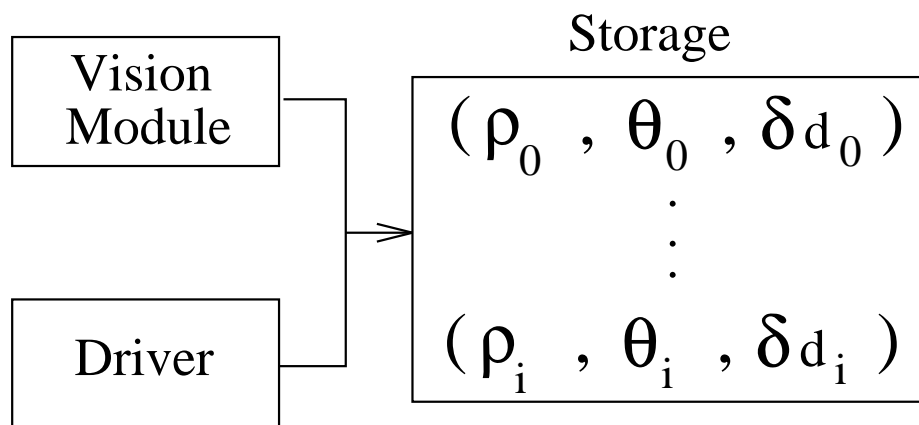


Figure 48: Data storage (step 1)

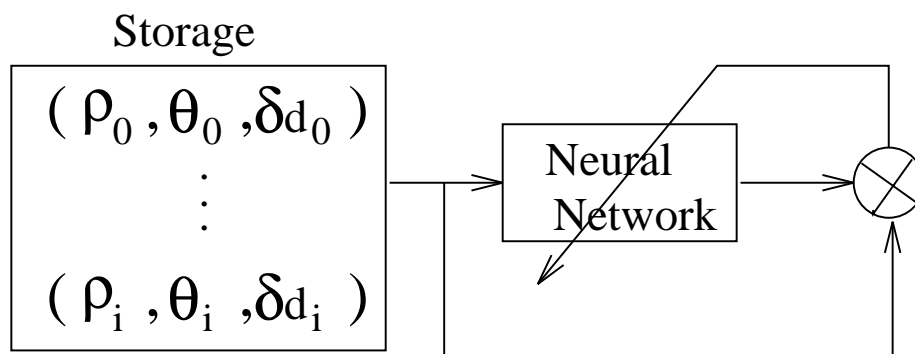


Figure 49: Learning set creation (step 2)

Results of learning

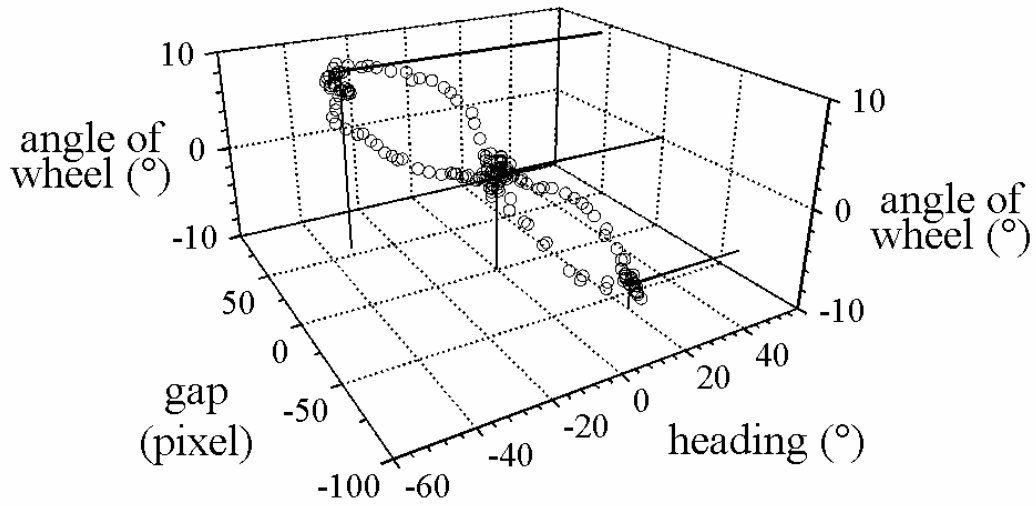


Figure 50: Learning set $(\rho_i, \theta_i, \delta_i)$

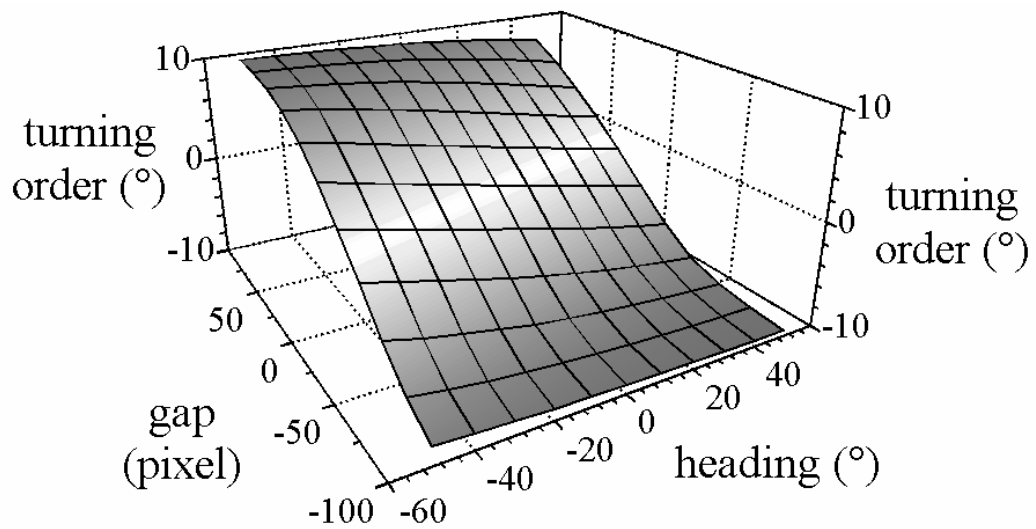


Figure 51: Off-line learning result

4.4 Experimental Results

4.4.1 Implementation Considerations

In order to test our three control laws, we laid out a trajectory composed of a bend, a step of one meter and a straight line.

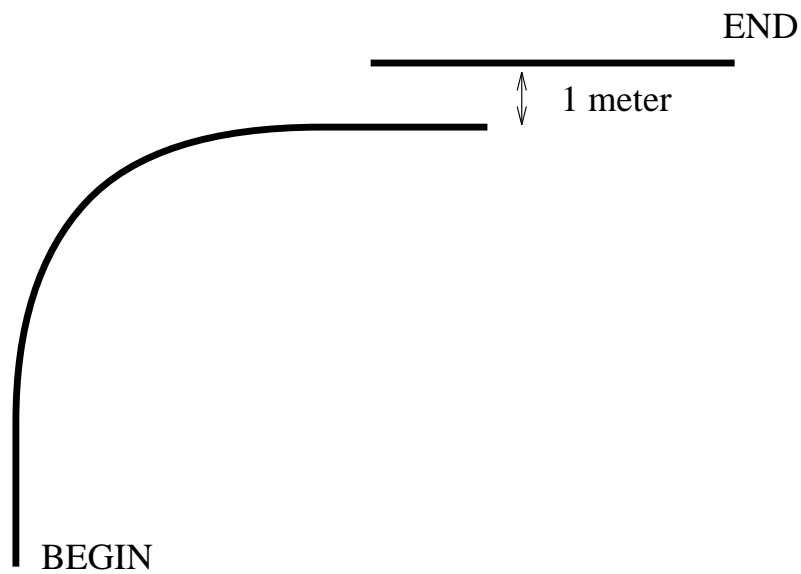


Figure 52: Diagram of the test track

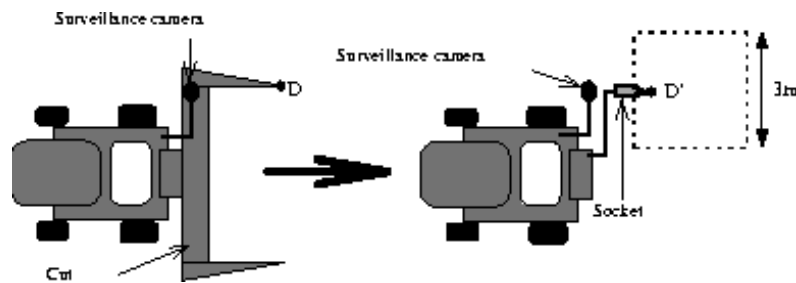


Figure 53: Replacing the cut by a socket

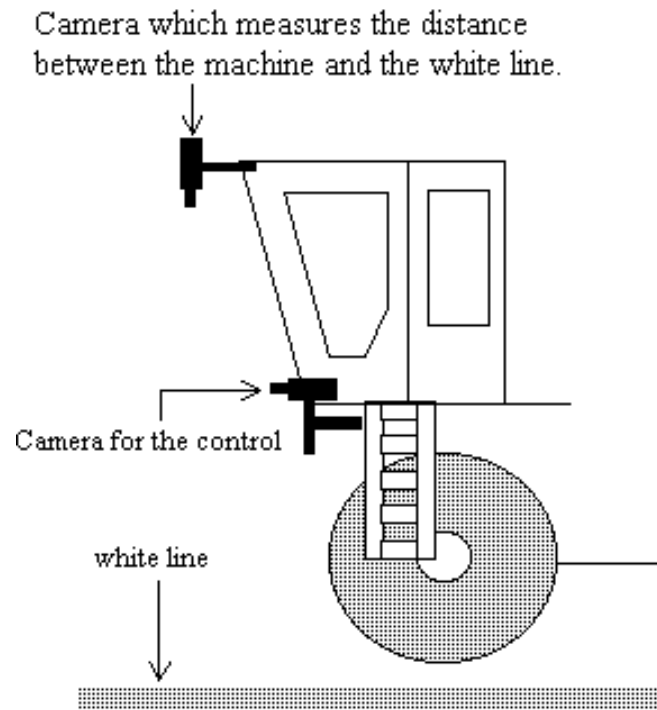


Figure 54: Camera positioning

- the first camera supplies an image of the white line
- the second camera measures the quality of our control laws accuracy (of ± 5 cm)

For each control law, we carried out the same tests under the same conditions :

- following the trajectory at several speeds
- adding noise to the visual informations (± 16 pixels in ρ)

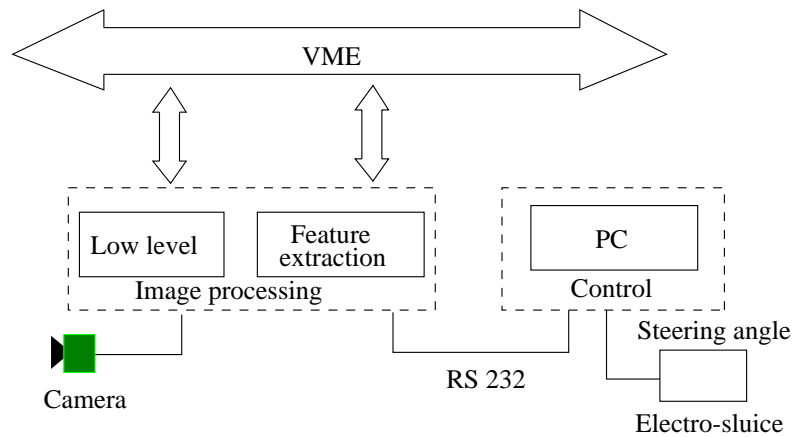


Figure 55: Parallel architecture

- architecture composed of two VME microprocessor boards
- three parts : a low level module, a feature extraction module and a control module
- OS9 operating system
- the image processing calculation time is about 200 ms (close to that encountered in a natural environment)
- a personal computer controls the steering angle

4.4.2 First Law

$\omega_0(rd/s)$	ξ	$V(km/h)$
0.14	0.9	4

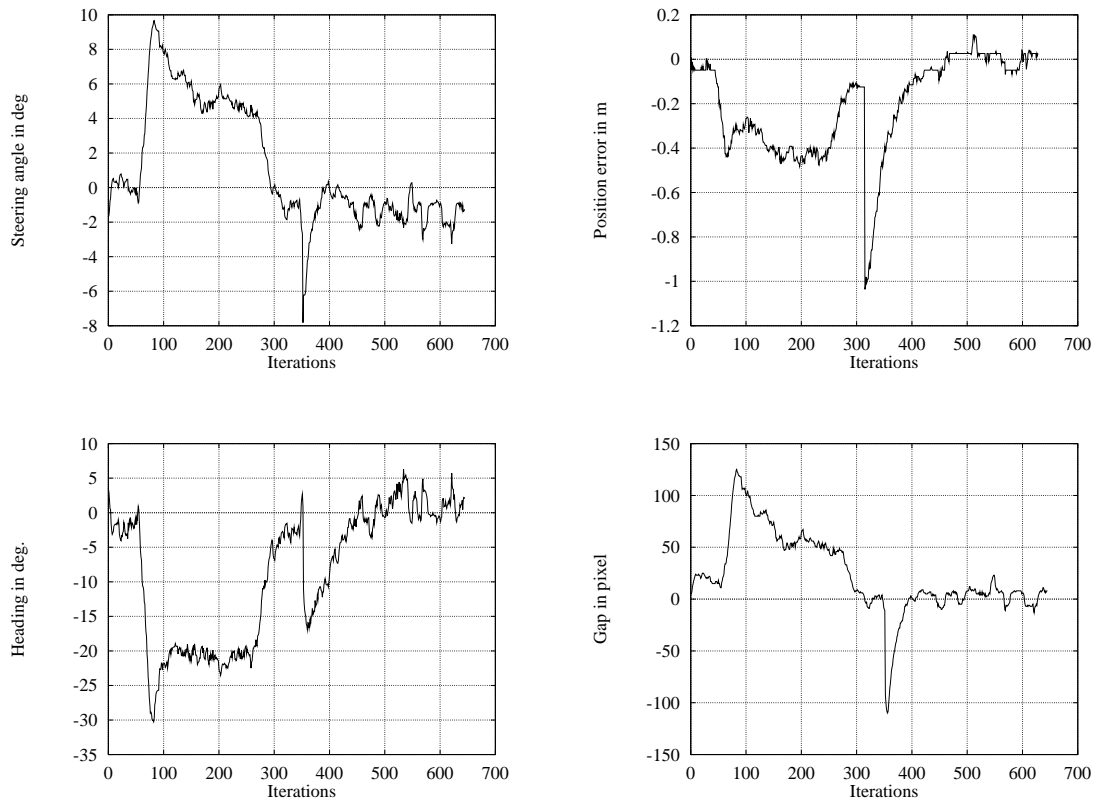


Figure 56: Test at 4 km/h ($\xi = 0.9$, $\omega_0 = 0.14rd/s$)

The control gains are adjusted the average speed $V = 4$ km/h. The results concern :

- the input δ and the lateral position x of the machine
- the features errors θ and ρ

$\omega_0 (rd/s)$	ξ	$V (km/h)$
0.14	0.9	4

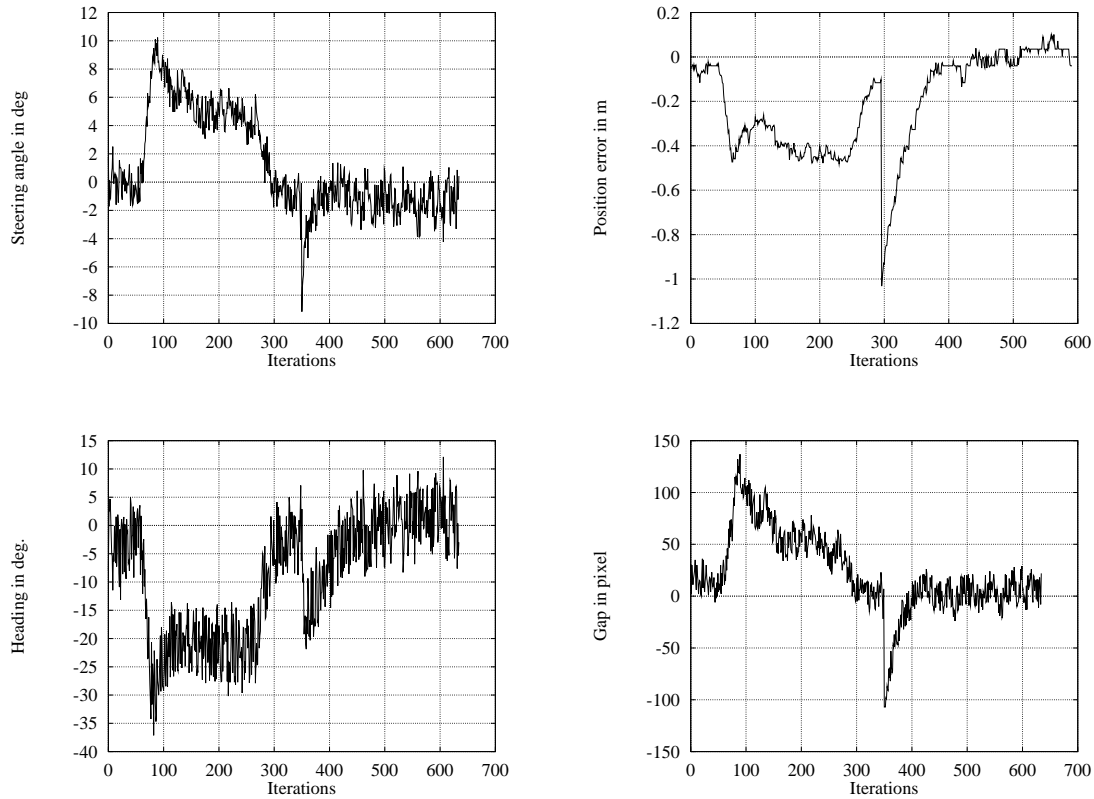


Figure 57: Test at 4 km/h with 16 pixels of noise in ρ

- test of the robustness of the control law
- the servoing task is achieved with good stability and robustness

$\omega_0 (rd/s)$	ξ	$V (km/h)$
0.14	0.9	4

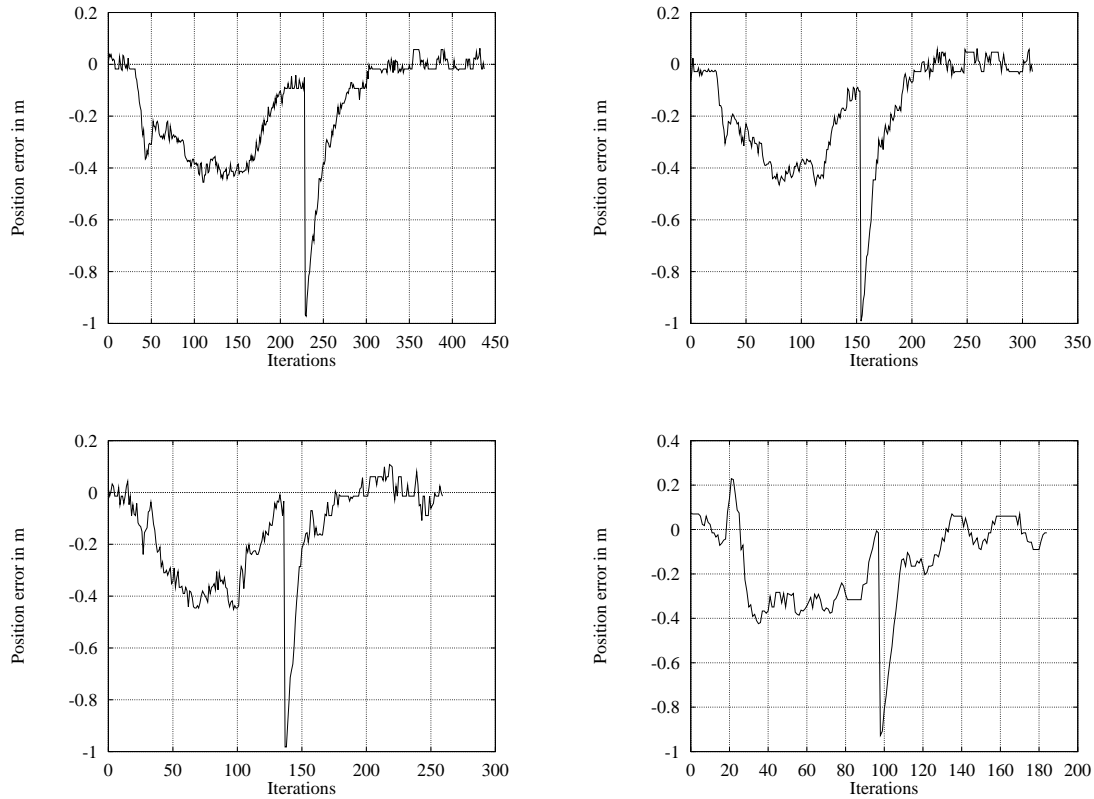


Figure 58: Test with $V = 6, 8, 10$ and 13 km/h)

- the gain control are evaluated for $V = 4$ km/h
- the machine is moved at different velocities (6, 8, 10 and 13 km/h)
- increasing speed causes the controlled behaviour to oscillate at steady-state

4.4.3 Second Law

λ	β	$V(km/h)$
0.3	2.6	4

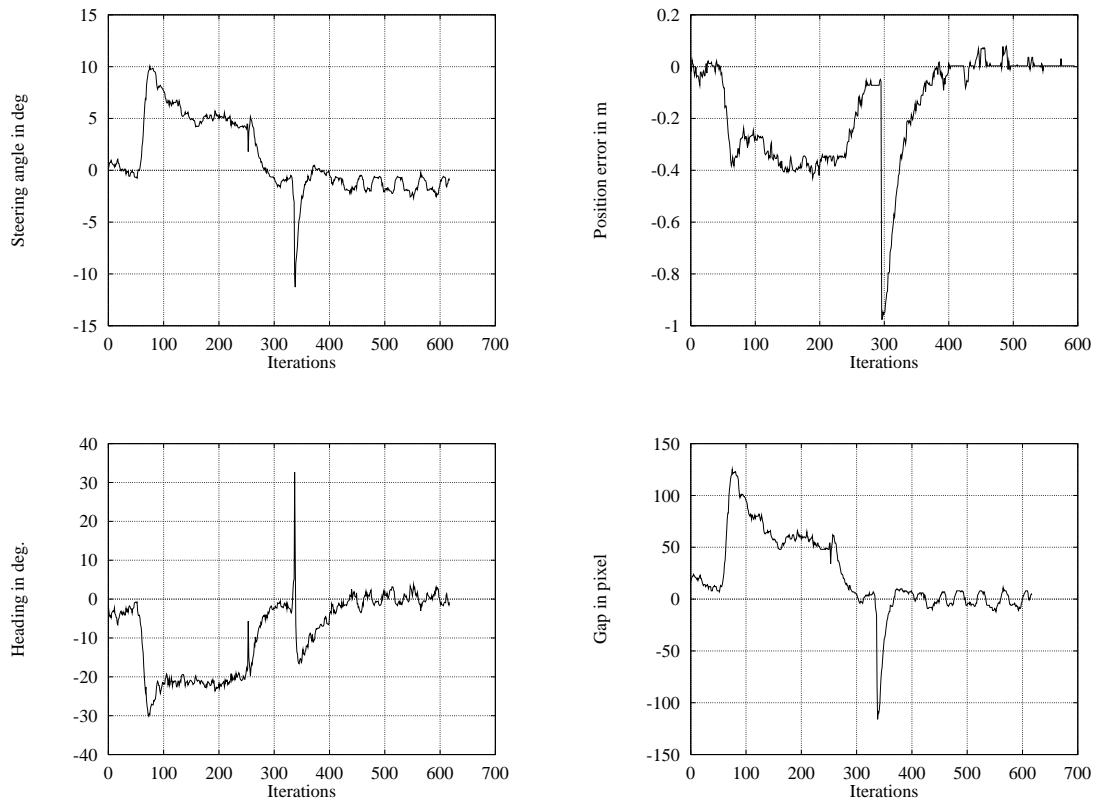


Figure 59: Test at 4 km/h

- results shown are obtained at a speed of 4 km/h
- response time is about 20 s with no overshooting

λ	β	$V(km/h)$
0.3	2.6	4

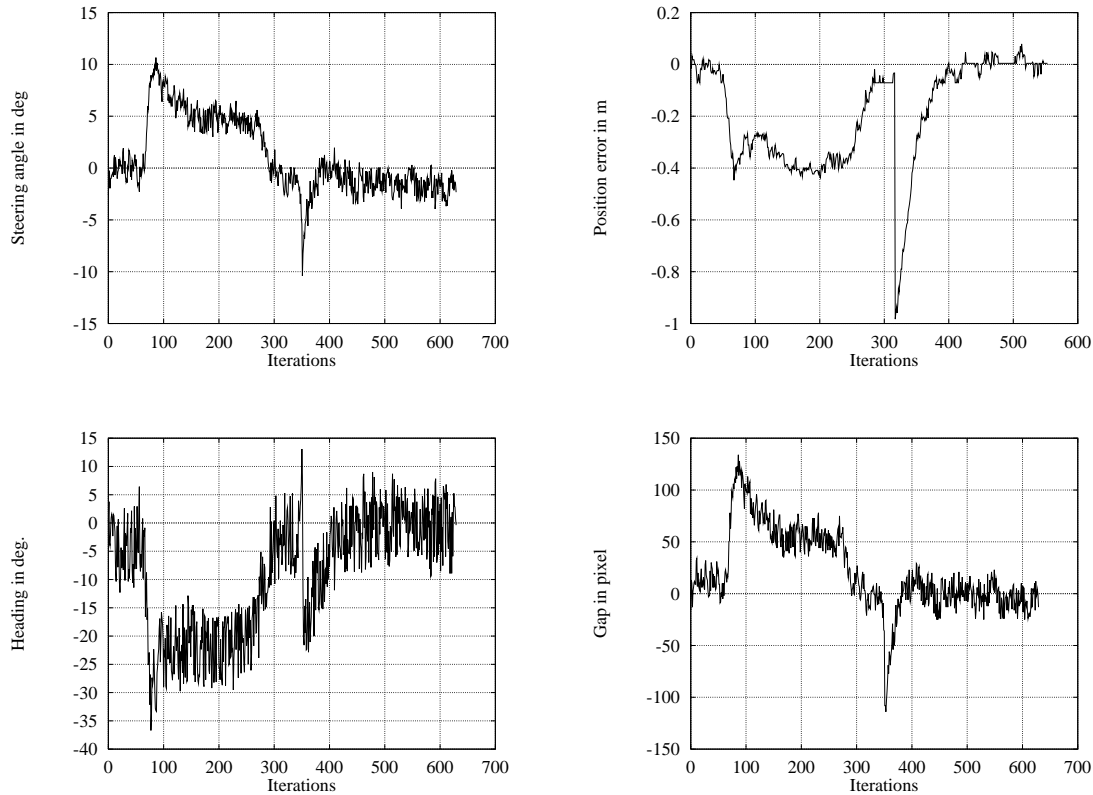


Figure 60: Test at 4 km/h with 16 pixels of noise in ρ

- noise has few consequence on our system
- the same remark as for the first law

In fact, the noise of the algorithm which is used to control the quacity of our system has more consequences than the effect of noise introduced in the result of the image processing.

λ	β	$V(km/h)$
0.3	2.6	4

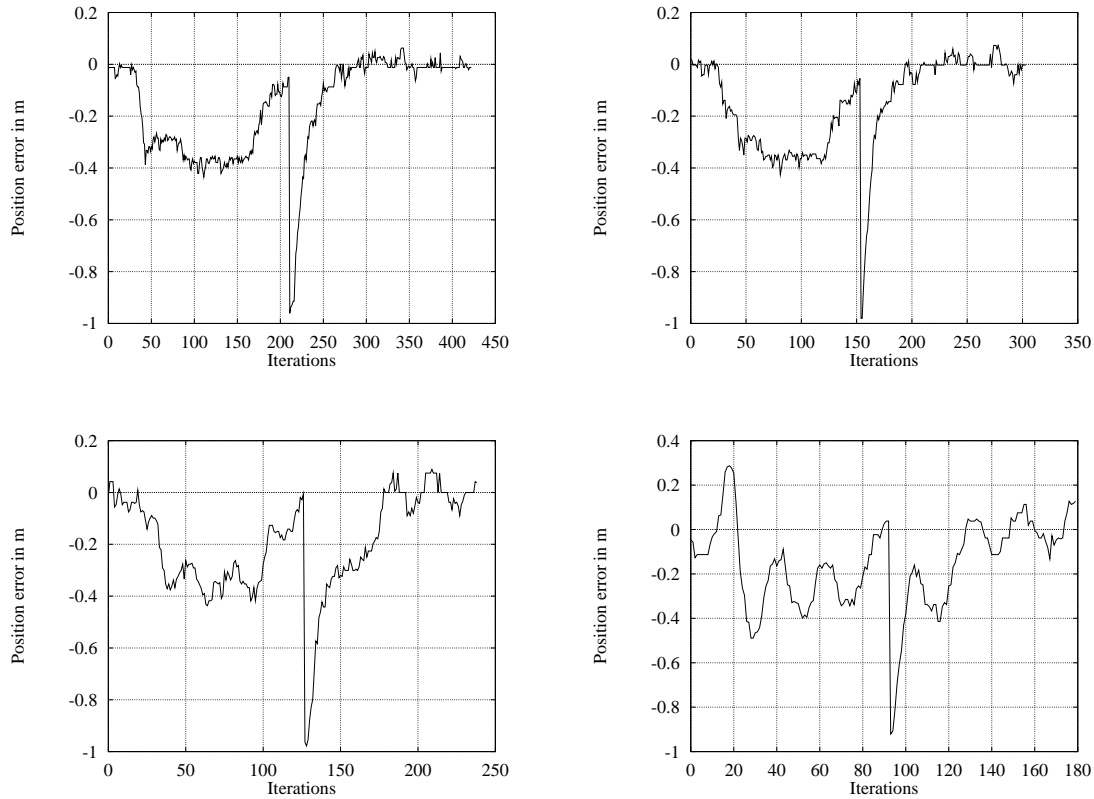


Figure 61: Test with $V= 6, 8, 10$ and 13 km/h)

- the response of the machine is reduced (inverse of V)
- the same results when the speed V increases

4.4.4 Third Law (neural approach)

The learning phase was carried out at a velocity of 4 km on a learning track different from the test track (in particular, the radius of the bend is large).

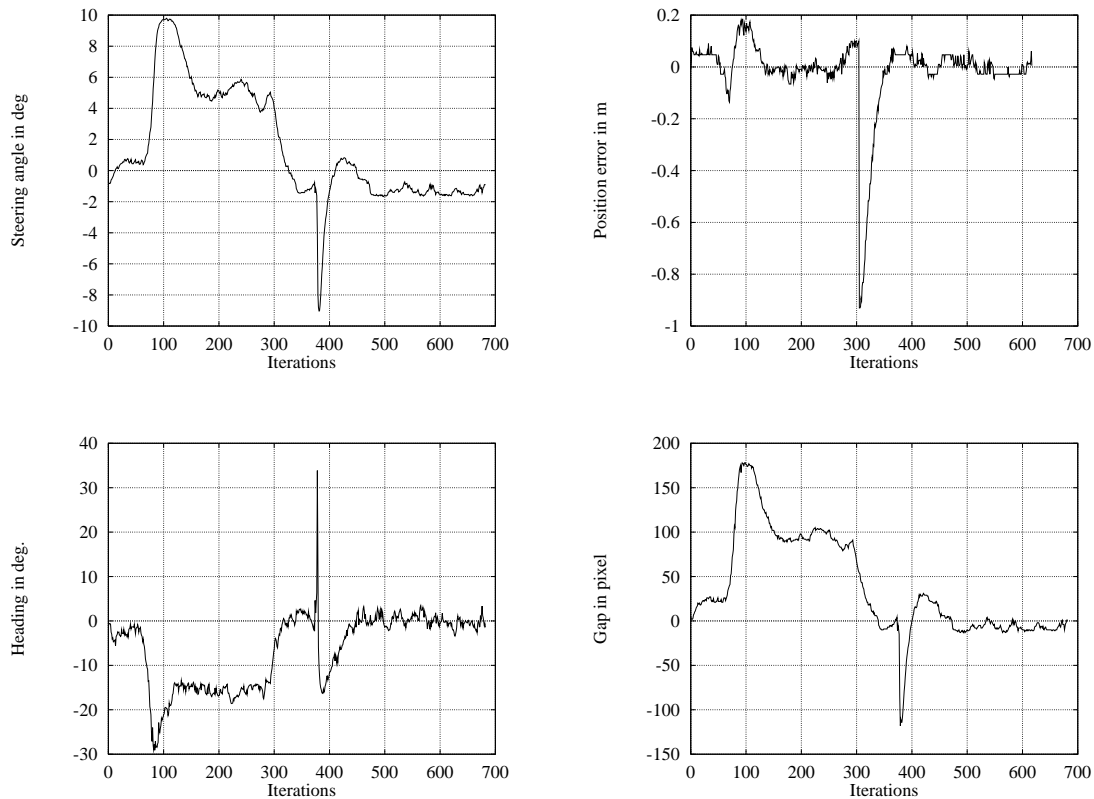


Figure 62: Test at 4 km/h

- close conditions as in learning
- the machine follows the track with good stability

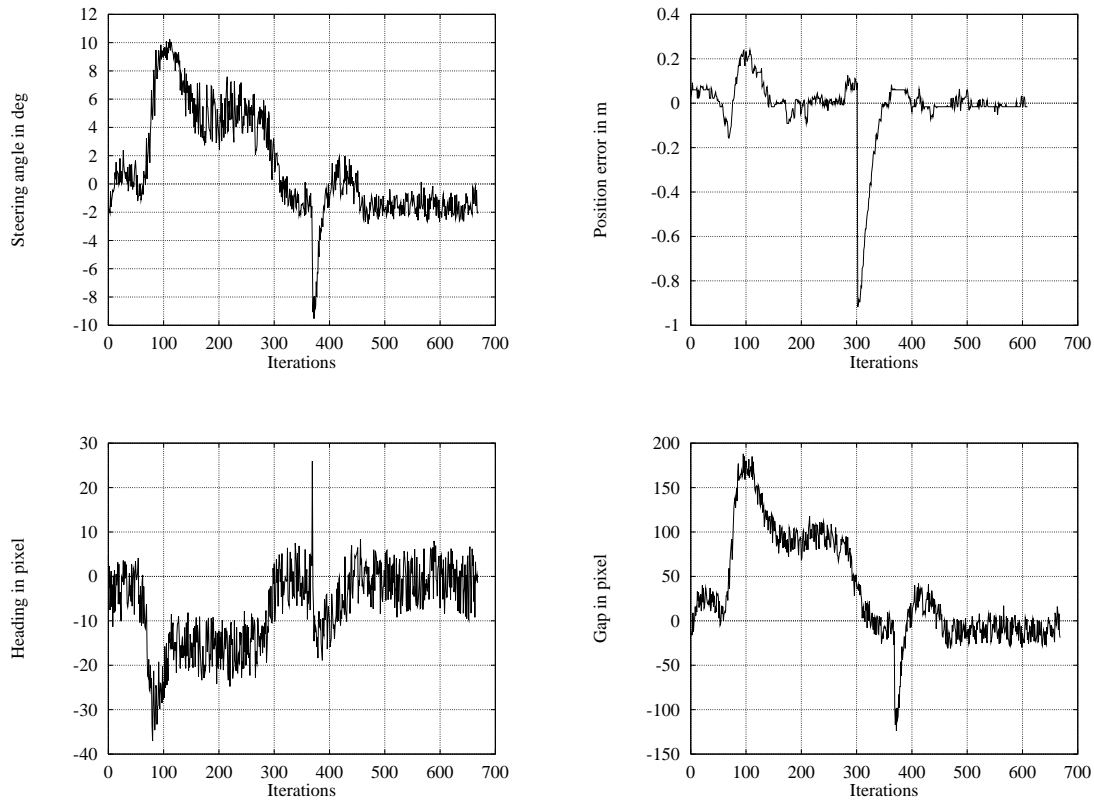


Figure 63: Test at 4 km/h with 16 pixels of noise in ρ

- no effect on the performance of the vehicle behavior
- the machine itself constitutes a natural filter for the turning orders

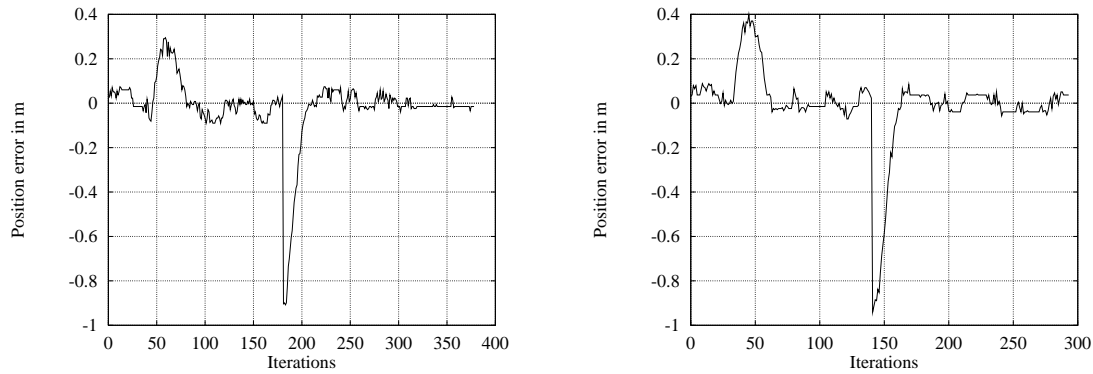


Figure 64: Test with $V = 6, 8$ km/h)

- a small performance degradation at the beginning of the bend, when the speed increases
- an overshoot of 18 cm at 4 km/h, 25 cm at 6 km/h and 39 cm at 8 km/h.
- test with a higher speed leads to oscillations and divergence

4.4.5 Conclusion

We have presented a system that provides the driving assistance to an agricultural mobile machine in order to help human beings in repetitive and difficult tasks in a natural environment.

The system is based on a vision system using a single camera. Three vision-based control laws were tested successfully. For each law, the control is directly specified in terms of regulation in the image space.

Law by Law...:

- First law
 - need of the interaction matrix (scene modelling)
 - need of the vehicle model (kinematic only)
 - adaptive control gains (V , and time response)
 - results show good convergence and the robustness
 - extension for any other steerable, mobile, wheeled robot
 - not react correctly in the case of a sharp bend
 - the regulation is done in movement (-)

- Second law:
 - need of the interaction matrix (scene modelling)
 - need of the vehicle model (kinematic only)
 - need a phase of empirical gain research
 - results show good convergence and the robustness
 - extension for any other machines whose trajectory at constant speed is a circle
 - not react correctly in the case of a sharp bend
 - the regulation is done in movement (-)

- Third law:
 - “black-box modelling” method
 - need a phase learning
 - results show good convergence and the robustness
 - automatic guidance system rivals a human driver in performance
 - react correctly in the case of a sharp bend
 - extension for any other machines
 - do not react correctly at increasing speed

4.5 Guiding the vehicle on a slope ground

The aim is :

- to guide the combine on a slope ground as well as on a flat ground
- to use the task function approach (sensor space)
- to only use the vision sensor

For that, we propose:

- to analyse the effect of the slope ground :
 - on the vehicle behavior
 - on the sensor signal behavior
- to adapt the control law:
 - using of a PI controller
 - adding an adaptative module in the visual servoing scheme

Slope ground:

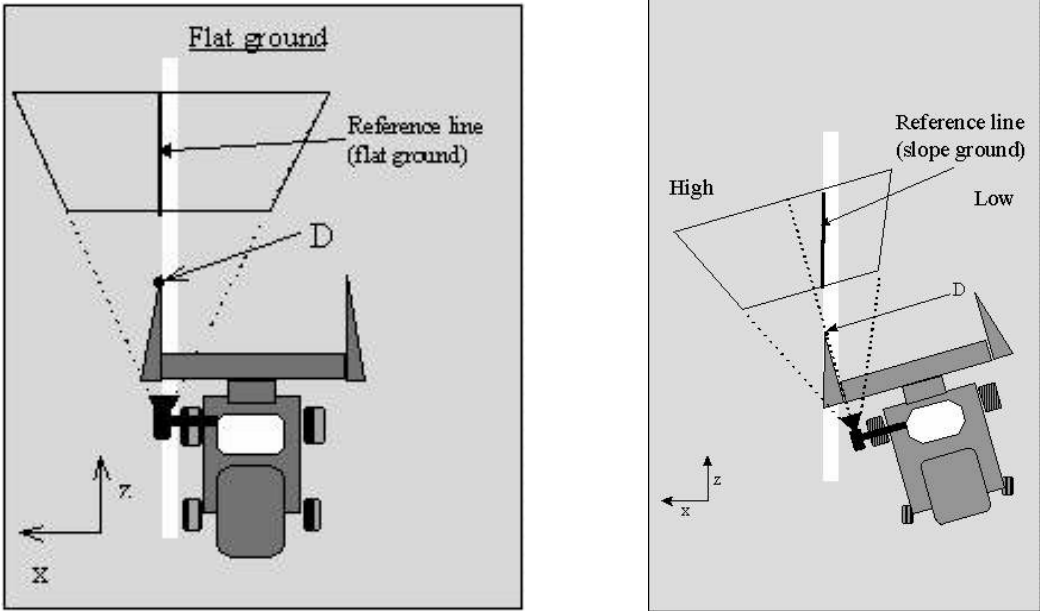


Figure 65: Flat ground and Slope ground effect

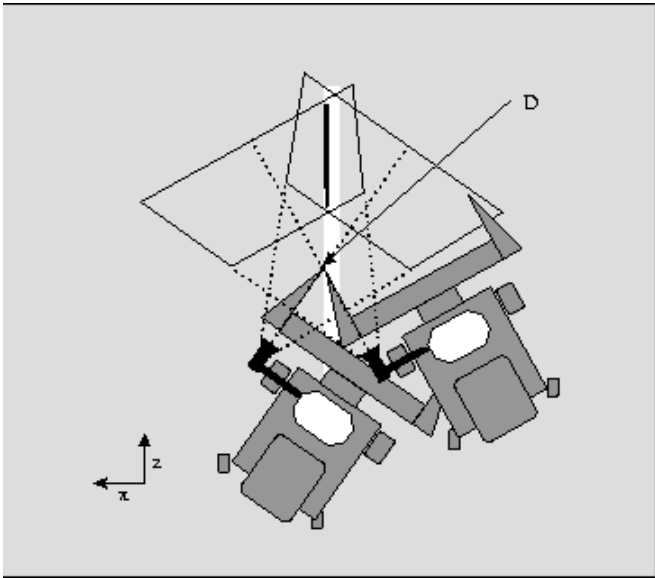


Figure 66: Steady state error in presence of slope ground

Simulation results on a slope ground

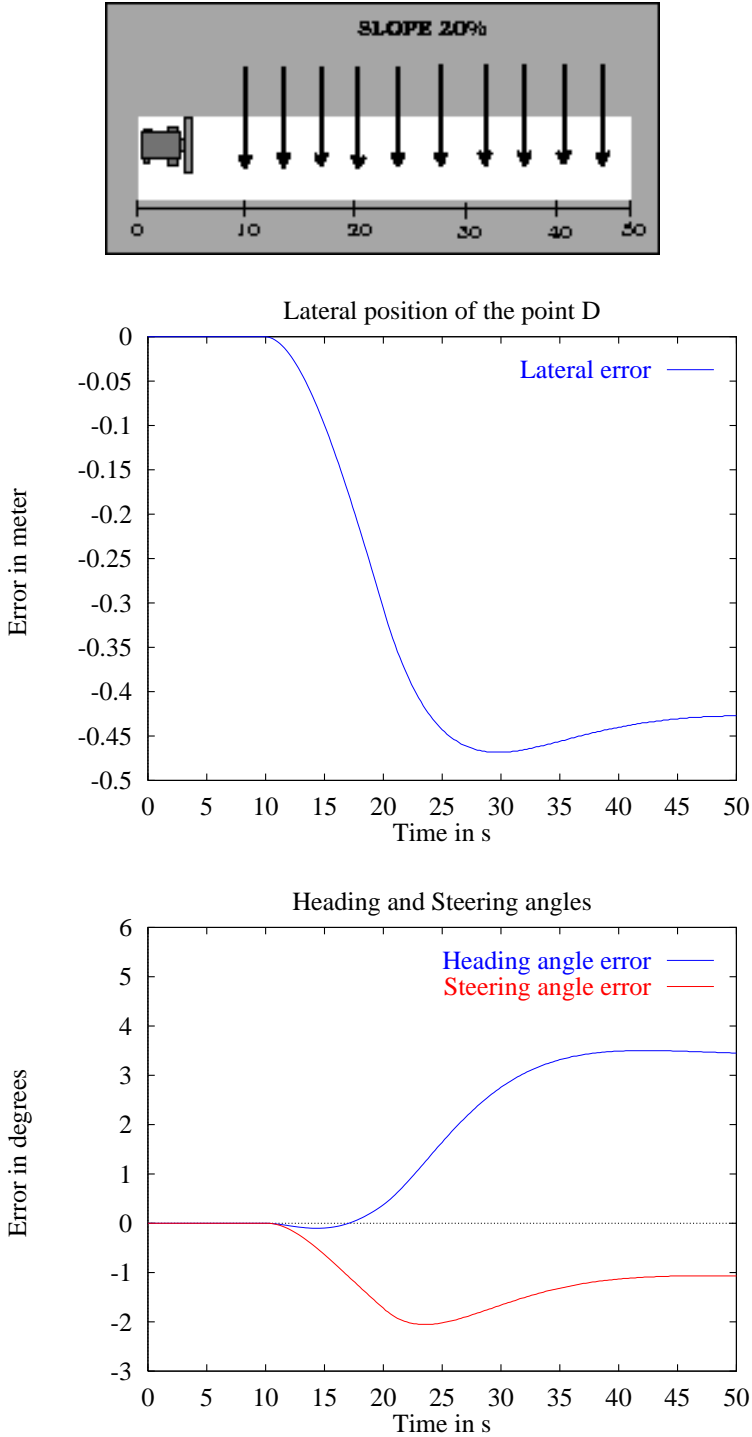


Figure 67: Simulation of slope (20%)

An adaptative control strategy

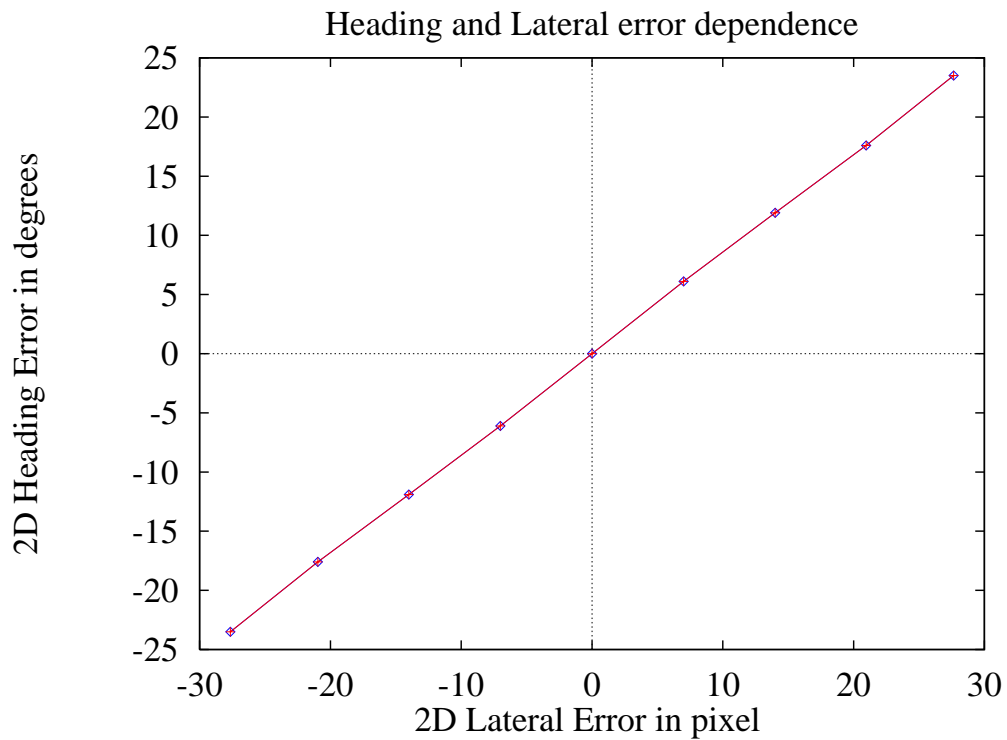


Figure 68: Adaptive reference signal graph

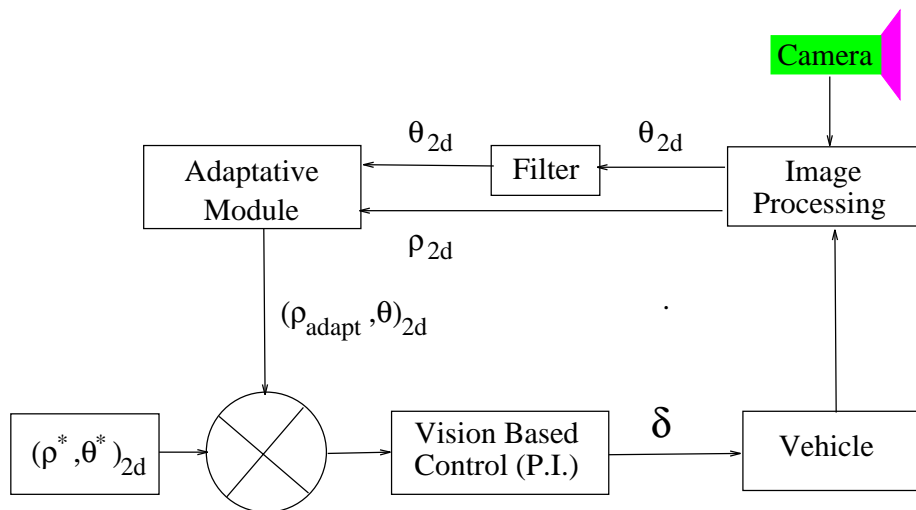


Figure 69: Adaptive visual servoing scheme

Using the second control law with $(\theta^*, \rho^*)^t = (0, 0)^t$, we have :

$$\delta = -\frac{\lambda L}{V} \left[\beta \frac{\sin \alpha \cos \alpha}{1+h^2} \theta - \frac{h^2 + \cos^2 \alpha}{1+h^2} \rho \right] \quad (56)$$

Using an integrator in the control law :

$$\delta = -\frac{\lambda L}{V} \left[\beta \frac{\sin \alpha \cos \alpha}{1+h^2} (\theta + k_1 \cdot \int_0^t \theta du) - \frac{h^2 + \cos^2 \alpha}{1+h^2} (\rho + k_2 \cdot \int_0^t \rho du) \right] \quad (57)$$

According to the previous graph, we use:

$$(k_1, k_2)^t = (0, k_2)^t.$$

Finally, the control law used on a slope ground becomes :

$$\delta = -\frac{\lambda L}{V} \left[\beta \frac{\sin \alpha \cos \alpha}{1+h^2} \theta - \frac{h^2 + \cos^2 \alpha}{1+h^2} (\rho_{adapt} + k_2 \cdot \int_0^t \rho_{adapt} du) \right] \quad (58)$$

Simulation results on slope ground

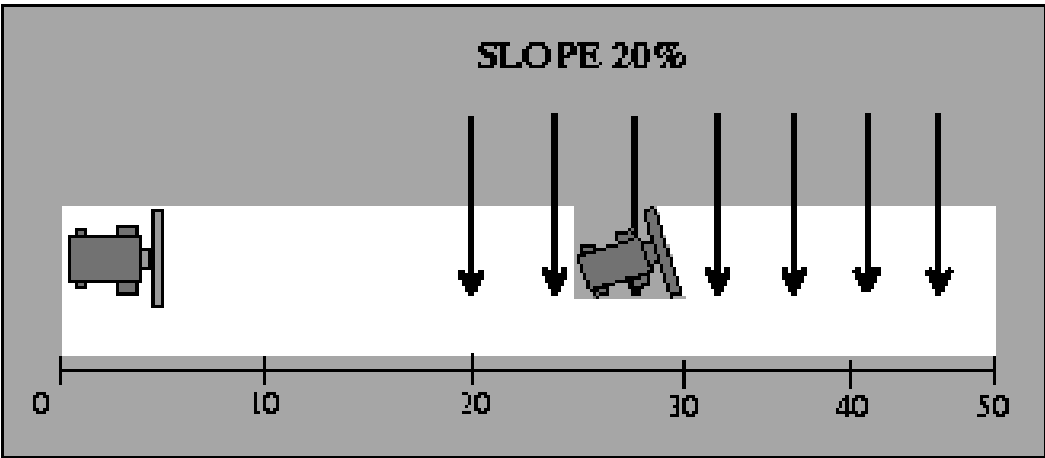


Figure 70: Simulation of slope (20%)

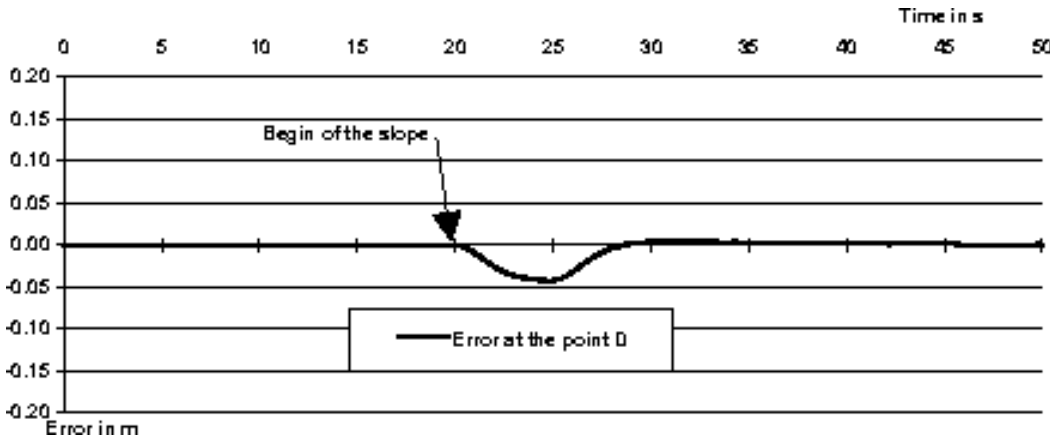


Figure 71: Result of simulation

Real experimentation on slope ground



Figure 72: Real experimentation

5 Conclusion and Perspectives

- Conclusion:
 - sensing in real environment remain difficult
 - a complete scene modeling in natural environment is difficult
 - an alternative way is to generate trajectory in a local environment (even if the experimental results for the lawn mower are not so good)
 - another way is use the sensor space, and the task function approach
 - another way is use the sensor space, and the neural network approach

- Perspectives:
 - develop the modeling of the slope ground and its dynamic effects
 - use of GPS/DGPS system apply in agricultural field

DGPS system apply in agricultural field

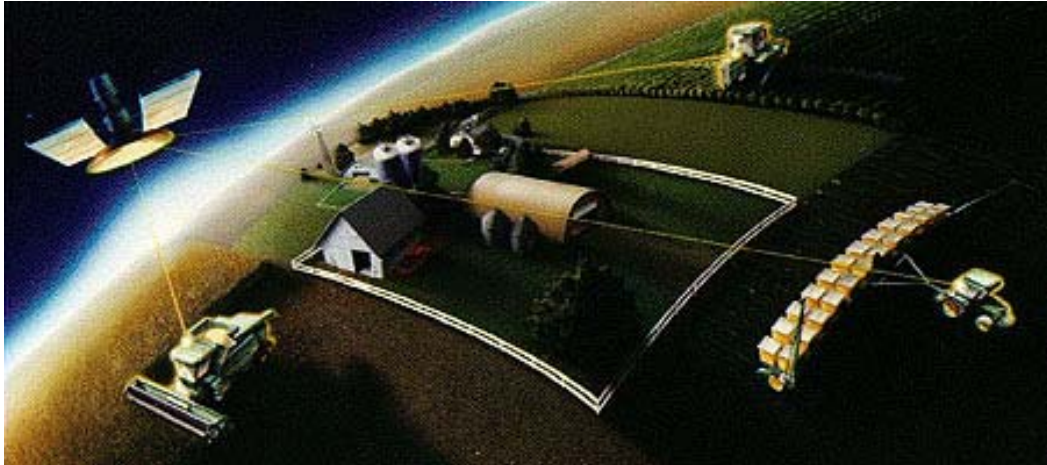


Figure 73: GPS/DGPS system (*John Deere*)

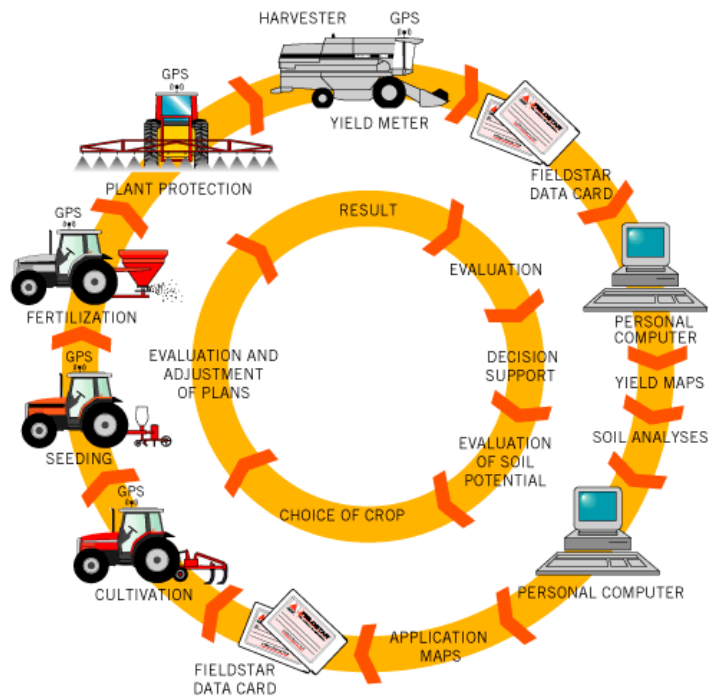


Figure 74: GPS/DGPS system (*Case*)

6 Video

Image Processing Architecture

The land mower (natural environment)

The combine harvester (test bed environment)

The combine harvester (slope ground)

The combine harvester (natural environment)

References

- [ABFM93] J. Amat, J. Battle, J.M. Fuertes, and A.B. Martinez. Vision controlled robot for agricultural application. In *24th ISIR*, pages 537–542, November 4-6 1993.
- [AS91] M. Abbassi and M.R. Sayed. Class of learning algorithms for multilayer perceptron. In *Proceedings of the SPIE*, pages 237–242. International Society for Optical Engineering, 1991. vol.1396.
- [CAG92] A. Casals, J. Amat, and A. Grau. Texture parametrization method for image segmentation. In *Proceedings of Second European Conference on Computer Vision ECCV'92*, pages 160–164, May 1992.
- [Cha90] F. Chaumette. *La relation vision-commande : théorie et application à des tâches robotiques*. PhD thesis, IRISA/INRIA-Rennes, Rennes, France, July 1990.
- [CRE91] F. Chaumette, P. Rives, and B. Espiau. Positioning of a robot with respect to an object, tracking it and estimating its velocity by visual servoing. In *proceedings of the IEEE, International Conference on Robotics and Automation*, pages 2248–2253, Sacramento, California, April 1991.
- [Day90] J. Dayhoff. *Neural Network Architectures : an introduction*, chapter The exclusive or : a classic problem. VNR Press, 1990.

- [DBB91] M. Derras, M. Berducat, and P. Bonton. Vision guided mower for the upkeep of natural environment. In *Proceedings of the 1st International seminar of on-machine vision systems for the agricultural and bio-industries*, pages 37–46, Montpellier, september 1991.
- [DBB⁺93] M. Derras, M. Berducat, P. Bonton, J. Gallice, and R. Canals. Segmentation texturale originale appliquée au guidage visuel d’un robot d’entretien d’espaces naturels. In *14^{ème} colloque sur le traitement du signal et des images*, pages 771–778. GRETSI, Juan-les-Pins-France, Sptember 1993.
- [DDB⁺94] C. Debain, M. Derras, M. Berducat, P. Bonton, and J. Gallice. Development of a visual guidance system for an upkeep robot of natural environments. In *International Symposium on Signal Processing, Robotics an Neural Networks*, pages 121–124. IMACS, Lille-France, April 1994.
- [Deb96] C. Debain. *Lois de commande pour le contrôle et la mobilité de machines agricoles*. PhD thesis, Blaise-Pascal, Clermont-Ferrand, France, september 1996.
- [Der93] M. Derras. *Segmentation non supervisée d’images texturées par champs de Markov : Application à l’automatisation de l’entretien des espaces naturels*. PhD thesis, Blaise-Pascal, Clermont-Ferrand, France, December 1993.
- [DVBB95] M. Derras, L. Verrat, M. Berducat, and P. Bonton. Image processing and algorithms merging :

Real time control of an upkeep machine for natural spaces. In *Fourth Workshop on Robotics in Agriculture and the Food-Industry*, pages 93–98, October 1995.

- [ECR92] B. Espiau, F. Chaumette, and P. Rives. A new approach to visual servoing in robotics. *IEEE Transactions on Robotics and Automation*, 8(n.3), 1992.
- [Fau93] O. D. Faugeras. *Three Dimensionnal Computer Vision : Geometric Viewpoint*. 1993.
- [GGGD90] D. Genam, S. Genam, C. Graffigne, and P. Dong. Boundary detection by constrained optimization. *IEEE Transaction on Pattern Analysis and Machine Intelligence*, 12,(7):609–628, july 1990.
- [HHC96] G.D. Hager, S. Hutchinson, and P. Corke. *Visual Servo Control*. IEEE International Conference on Robotics and Automation, Minneapolis Hilton and Towers, Minneapolis, Minnesota, April 1996. Tutorial TT3.
- [HTC86] C.A. Harlow, M. Trivedi, and R.W. Connors. Use of texture operators in segmentation. *Optical Engineering*, 25(11):1200–1206, november 1986.
- [IBT88] E. Ioos, M. Bouille, and P. Tournassoud. Etude d’un sous-système de navigation pour un robot mobile. Technical Report 783, INRIA, INRIA Rocquencourt, France, Février 1988.
- [IHBHN89] J.M. Mc Inerney, K.G. Haines, S. Biafore, and Hecht-NielsenR. Error surfaces of multi-layer

networks can have local minima. Technical Report 157, CS89, 1989.

- [Jar90] R.A. Jarvis. Omniscient camera based outdoor mobile robot. In *Workshop on Robotics in Agriculture and the Food Industry*, pages 247–258,. 1st IARP, Avignon-France, 1990.
- [JRGJ94] F. Jurie, P. Rives, J. Gallice, and J.L.Brame. High-speed vehicle guidance based on vision. *Control Eng. Practice*, 2,(2):287–297, 1994.
- [Kel94] A. Kelly. A partial analysis of the high speed autonomous navigation problem. Technical report, The Robotics Institute Carnegie Mellon University, May 1994.
- [KGL91] N. Kehtarnavaz, N.C. Grisworld, and J.S. Lee. Visual control for an autonomous vehicle (bart)-the vehicle following problem pr. *IEEE Transactions on Vehicular Technology*, 40(3):654–662, August 1991.
- [KMG95] D. Khadraoui, P. Martinet, and J. Gallice. Linear control of high speed vehicle in image space. In *Second International Conference on Industrial Automation*, pages 517–522. IAIA, Nancy-France, June 1995.
- [KMM⁺96] D. Khadraoui, G. Motyl, P. Martinet, J. Gallice, and F. Chaumette. Visual servoing in robotics scheme using a camera/laser-stripe sensor. *IEEE Transactions on Robotics and Automation*, 12(5), October 1996.
- [KWW94] N.D. Klassen, R.J. Wilson, and J.N. Wilson. Guidance systems for agricultural vehicles. In

12th *World Congress on Agricultural Engineering*, pages 1136–1142. International Commission of Agricultural Engineering, Milano-Italia, August 29-September 1st 1994.

- [Le 87] Y. Le Cun. *Modèles connexionnistes d'apprentissage*. PhD thesis, Paris 6, Paris, France, June 1987.
- [MS93] R.M. Murray and S.S. Sastry. Nonholonomic motion planning : steering using sinusoids. *IEEE Transactions on Automatic Control*, 38(5):700–716, May 1993.
- [MSBHN89] J.M. Mc-Inerney, K.G. Haines S., Biafore, and R. Hecht-Nielsen. Error surfaces of multi-layer networks can have local minima. Technical Report CS 89-157, UCSD, CA, 1989.
- [Nob90] I. Nobutaka. Agricultural robots applications in japan. In *Proc. of IARP Workshop on Robotics in Agriculture and Food Industry*, pages 35–44, 1990.
- [OS96] M. Ollis and A. Stentz. First results in vision based crop line tracking. In *IEEE International Conference on Robotics and Automation*, pages 951–956, Minneapolis, Minesota, USA, April 1996.
- [Pau82] R. P. Paul. *Robot Manipulators : Mathematics, Programming, and Control*. MIT Press - Massachusetts Institute of Technology, Cambridge, Massachusetts 02142, 1982.
- [PR91] R. Pissard-Gibollet and P. Rives. Asservissement visuel appliqué à un robot mobile: état

de l'art et modélisation cinématique. Technical Report 1577, Rapport de recherche INRIA, Décembre 1991.

- [Ra86] D. Rumelhart and al. *Parallel and Distributed Processing*. MIT Press, 1986.
- [SBE91] C. Samson, M. Le Borgne, and B. Espiau. *Robot Control. The task function approach*. ISBN 0-19-8538057. Oxford, 1991.
- [SBMZ90] G. Sandini, F. Buemi, M. Massa, and Zucchini. Visually guided operations in green houses. In *Workshop on Robotics in Agriculture and the Food Industry*, pages 69–84. 1st IARP, Avignon-France, 1990.
- [SCZD94] F. Sevilla F., N. Clavel, R. Zapata, and E. Dubreuil. Perception, navigation et pilotage de machines mobiles en environnement rural. In *Revue d'automatique et de productique appliquée*, pages 339–363. , 3,1994.
- [Sul90] J.R. Sullins. Distributed learning of texture classification. In *ECCV 90*, pages 349–358, Antibes, 1990. European Conference on Computer Vision.